THE V-GROOVE LENS

A THESIS
SUBMITTED TO THE DEPARTMENT OF
ELECTRICAL AND ELECTRONICS ENGINEERING
AND THE INSTITUTE OF ENGINEERING AND SCIENCES
OF BILKENT UNIVERSITY
IN PARTIAL FULFILLMENT OF THE REQUIREMENTS
FOR THE DEGREE OF
MASTER OF SCIENCE

By
Ayhan Bozkurt
September 1994

THE V-GROOVE LENS

A THESIS

SUBMITTED TO THE DEPARTMENT OF ELECTRICAL AND

ELECTRONICS ENGINEERING

AND THE INSTITUTE OF ENGINEERING AND SCIENCES

OF BILKENT UNIVERSITY

IN PARTIAL FULFILLMENT OF THE REQUIREMENTS

FOR THE DEGREE OF
MASTER OF SCIENCE

By

Ayhan Bozkurt

September 1994

Ayhan Bozkurt

tarcf.n.:.. ... ;.......şir.
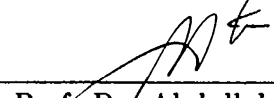
I certify that I have read this thesis and that in my opinion it is fully adequate, in scope and in quality, as a thesis for the degree of Master of Science.
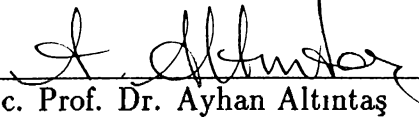
Prof. Dr. Abdullah Atalar(Supervisor)

I certify that I have read this thesis and that in my opinion it is fully adequate, in scope and in quality, as a thesis for the degree of Master of Science.
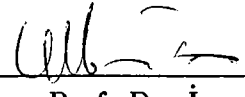
Prof. Dr. Hayrettin Köymen(Co-supervisor)

I certify that I have read this thesis and that in my opinion it is fully adequate, in scope and in quality, as a thesis for the degree of Master of Science.

Assoc. Prof. Dr. Ayhan Altıntaş

I certify that I have read this thesis and that in my opinion it is fully adequate, in scope and in quality, as a thesis for the degree of Master of Science.

Assoc. Prof. Dr. İrşadi Aksun

Approved for the Institute of Engineering and Sciences:

Prof. Dr. Mehmet Baray
Director of Institute of Engineering and Sciences

ii

ABSTRACT

THE V-GROOVE LENS

Ayhan Bozkurt
M.S. in Electrical and Electronics Engineering
Supervisors: Dr. Abdullah Atalar
and Dr. Hayrettin Köymen
September 1994

Primarily designed for imaging purposes, the acoustic microscope finds application in the qualitative evaluation of materials, too. The lens response as a function of defocus, which is known as the $V(z)$ curve, is formed by the interference of various wave components reflected from the material surface. Leaky wave velocities of the material can be extracted from this interference pattern. The accuracy of the measurement is heavily influenced by the leaky wave contribution to the $V(z)$ curve. Hence, lens geometries capable of efficiently exciting leaky wave modes need to be designed. If a particular geometry is to be used for measurements on materials exhibiting crystalographic anisotropies, it must be able to couple to modes only in a single direction, as well. The proposed V-Groove lens, combines the directional sensitivity of the Line Focus Beam lens and the efficiency of the Lamb Wave lens. The geometry is able to accurately measure the direction dependent leaky wave velocities of anisotropic materials. A new model based approach improves the accuarcy of the extracted velocities.

In this study, the V-Groove lens has been analyzed theoretically. A mathematical model describing the lens response has been developed. The performance of the V-Groove lens has been tested by simulations. A new leaky wave velocity extraction algorithm based on fitting the model curve to actual curves using Nelder-Meade search has been proposed. A prototype lens has been manufactured and performance figures have been verified experimentally. The accuracy of the lens has been compared with those of other various geometries.

Keywords : Acoustic microscopy, V-Groove lens, Line Focus Beam (LFB) Lens, Lamb Wave Lens, leaky waves, $V(z)$ curves.

ÖZET

V-OLUKLU MERCEK

Ayhan Bozkurt
Elektrik ve Elektronik Mühendisliği Bölümü Yüksek Lisans
Tez Yöneticileri: Prof. Dr. Abdullah Atalar
ve Prof. Dr. Hayrettin Köymen
Eylül 1994

Öncelikle malzeme görüntülenmesi amacıyla tasarlanmış olan akustik mikroskop, nicel gözlemler yapılmasında da kullanılmaktadır. Malzeme yüzeyinden yansıyan değişik dalga bileşenlerinin girişim yapması, malzeme ile mercek arasındaki uzaklıklığa bağlı bir mercek yanıtını, ya da bilinen adıyla $V(z)$ eğrilerini üretmektedir. Bu girişim deseninden malzemenin sızıntılı yüzey dalgası hızları belirlenebilmektedir. Ölçümün hassaslığı, sızıntılı dalga bileşenlerinin $V(z)$ eğrisine katkısıyla değişmektedir. Bu nedenle, bu dalga bileşenlerini etkili olarak uyarabilecek mercek biçimlerine gereksinim vardır. İzotropik olmayan kristal yapılı malzemelerin nicelenmesinde de kullanılacak bir merceğin, bunun dışında, sadece belli bir yöndeki dalga bileşenlerine güç aktarabilmesi gerekmektedir. Önerilen V-Oluklu mercek, Çizgi Odaklı Mercek'in yön duyarlığı ile Lamb Dalgası Merceği'nin verimliliğini birleştirmektedir. Bu geometri ile izotropik olmayan malzemelerin yöne bağlı sızıntılı yüzey dalgası hızları hassas olarak ölçülebilmektedir. Modele dayalı yeni bir yöntem, özütlenen dalga hızlarının kesinliğini iyileştirmektedir.

Bu çalışmada, V-Oluklu merceğin kuramsal çözümlemesi yapılmıştır. Mercek yanıtını matematiksel olarak açıklayan bir model geliştirilmiştir. Merceğin performansı benzeşimlerle sınanmıştır. Modelin ürettiği eğrinin Nelder-Mealde arama yöntemi kullanılarak gercek mercek yanıtına uydurulmasına dayalı yeni bir sızıntılı dalga hızı özütleme yöntemi önerilmiştir. Üretilen örnek mercekle benzeşim sonuçları deneysel olarak doğrulanmıştır. Mercekle yapılan ölçümlerin doğruluğu, diğer bazı mercek geometrilerininkiyle karşılaştırılmıştır.

Anahtar Kelimeler : Akustik mikroskop, V-Oluklu mercek, Çizgi Odaklı Mercek, Lamb Dalgası Merceği, sızıntılı yüzey dalgası, $V(z)$ eğrisi.

ACKNOWLEDGMENTS

TABLE OF CONTENTS

LIST OF FIGURES

ix

Chapter 1

INTRODUCTION

The acoustic microscope has proven itself to be powerful tool in ultrasonic imaging technology and found applications in the fields of biological science, material science and non-destructive evaluation. Since its first introduction by Lemons and Quate [2], improvements in the hardware [3] lead to resolutions comparable to that of optical systems. More than that, the penetration ability of acoustic waves, enabled the imaging of optically opaque materials. A major advance in acoustic microscopy has been achieved when it was found that the reflected signal amplitude from an acoustic lens varies with the lens-object spacing. Known as $V(z)$ curves [4], this unique mechanism due to the presence of leaky waves, contained information on the elastic parameters of the material under observation. Consequently, the acoustic microscope, besides being an imaging tool, became popular in the qualitative evaluation of material properties.

1.1 Qualitative Acoustic Microscopy of Anisotropic Crystal Materials

An acoustic lens to be used in the characterization of anisotropic materials has to have direction sensitivity, as leaky wave velocities are direction dependent for these materials. Furthermore, the efficiency of power coupling to a particular wave mode must be high for accurate measurements. This issue becomes more critical for high speed materials for which the number of oscillations in the $V(z)$ curves are limited. The conventional spherical lens, which was originally designed for imaging purposes, possesses neither of these properties: The lens insonifies the material surface at all incidence angles, exciting all possible wave

modes including bulk modes. Furthermore, due to the circular symmetry of the beam generated by the lens, the measured acoustic parameters turn out to be their mean values around the beam axis. Hence, the spherical lens cannot be used for materials that exhibit crystallographic anisotropies.

The line focus beam (LFB) lens, introduced by Kushibiki and Chubachi [5], solves the directivity problem and produces $V(z)$ curves by which the leaky wave velocity in a particular direction can be deduced with high accuracy. However, this geometry has efficiency problems due to coupling to undesired wave modes and the signal level in $V(z)$ curves decreases with increasing defocus. This degrades the measurement accuracy for materials with high leaky wave velocities. The Lamb wave lens, due to Atalar and Köymen [6], has the ability of exciting one particular mode at a time by generating conical wavefronts at a fixed incidence angle. With its efficiency, the Lamb wave lens maintains a large signal level at an extended defocus range. However, it does not have a directional sensitivity which is required for the characterization of anisotropic materials.
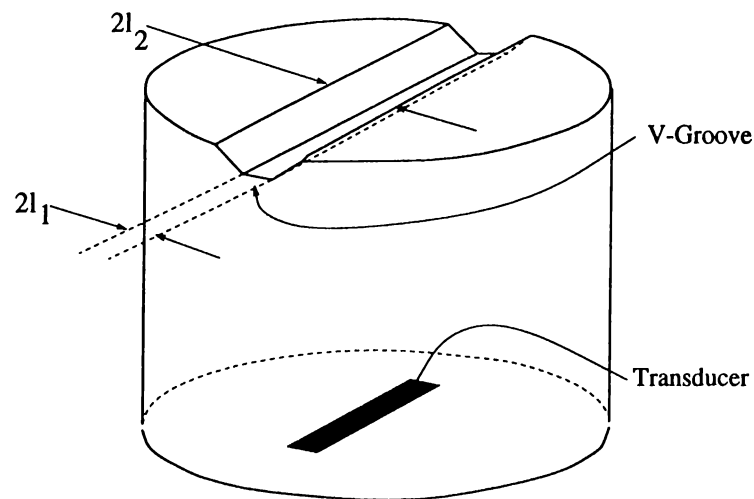
Figure 1.1: The V-groove lens.

The V-groove lens has emerged as a combination of the LFB lens and the Lamb wave lens [7]. Its cross-section is the same as that of the Lamb wave lens in one of the lateral directions, while the geometry remains the same in the traverse direction, rather than having circular symmetry. As depicted in fig. 1.1, the lens cavity resembles the letter V with a flat bottom, or literally, a groove. Essentially, the relationship between the LFB lens and the spherical lens is the same as that between the V-groove and Lamb wave lenses: being a directive version of the Lamb wave lens, the V-groove lens has the ability to selectively excite leaky wave modes, which is the missing feature with the LFB

2

lens due to its wide angular spectrum. Consequently, the V-groove geometry is very suitable for measurements on materials that have anisotropic nature. Fig. 1.2 depicts lens geometries discussed so far, together with an evaluation of their merits.

Name	: Spherical Lens
Primary Usage	: Imaging
Focusing properties:	Beam directivity ✗
	Mode selectivity ✗

Name	: Lamb-Wave Lens
Primary Usage	: Imaging
Focusing properties:	Beam directivity ✗
	Mode selectivity ✓

Name	: Line-Focus Beam Lens
Primary Usage	: Quantitative
Focusing properties:	Beam directivity ✓
	Mode selectivity ✗

Name	: V-Groove Lens
Primary Usage	: Quantitative
Focusing properties:	Beam directivity ✓
	Mode selectivity ✓

Figure 1.2: Lens geometries for acoustic microscopy.

The lens aperture is insonified by a rectangular transducer whose dimensions and spacing from the refracting element is adjusted for minimum waste of power. The field incident on the flat portion does not encounter any refraction, generating an obliquely incident beam on the material surface. The inclined side-walls of the groove, on the other hand, cause refraction, due to which two obliquely incident symmetrical beams are generated. These beams couple to leaky modes on the object surface when their median direction is close the critical angle of the material. The interference between these and the central beam produces the $V(z)$.

In this study, first a theoretical analysis of the V-groove lens is presented, explaining the $V(z)$ mechanism in detail, together with some design considerations. Then, the simulation program and the experimental set-up are described. Finally, results regarding the performance of the V-groove lens are presented.

3

Chapter 2

THEORY

The success of the acoustic microscope in the quantitative evaluation of materials is due to the $V(z)$ curves. The periodic dips and peaks appearing in these curves are generated by the interference of the acoustic beam that is specularly reflected from the liquid-material interface and the leaky waves excited on the surface of the material [8]. As it has been shown both theoretically and experimentally, $V(z)$ curves contain information from which the leaky wave velocity can be extracted. Physical models regarding this interference mechanism has been worked out by Parmon and Bertoni [9] and Atalar [10]. The motivation behind the determination of the leaky wave velocity is that, together with the acoustic attenuation values measured using the $V(z)$ curves, it enables a complete characterization of the material under observation.

2.1 Rayleigh Waves and Leaky Waves

Rayleigh waves are essentially a combination of shear and longitudinal stress components that are confined to the surface of a semi-infinite medium in vacuum. The solution of the acoustic wave equations yields the Rayleigh wave dispersion relation[11], namely,

$$\left(\frac{V_R}{V_s}\right)^6 - 8\left(\frac{V_R}{V_s}\right)^4 + 8\left[3 - 2\left(\frac{V_s}{V_l}\right)^2\right]\left(\frac{V_R}{V_s}\right)^2 - 16\left(1 - \frac{V_s}{V_l}\right)^2 = 0. \quad (2.1)$$

where V_l, V_s and V_R are the longitudinal, shear and Rayleigh wave velocities, respectively. Here, wave components are assumed to fall off exponentially into the semi-infinite medium as the surface wave has finite stored energy per unit
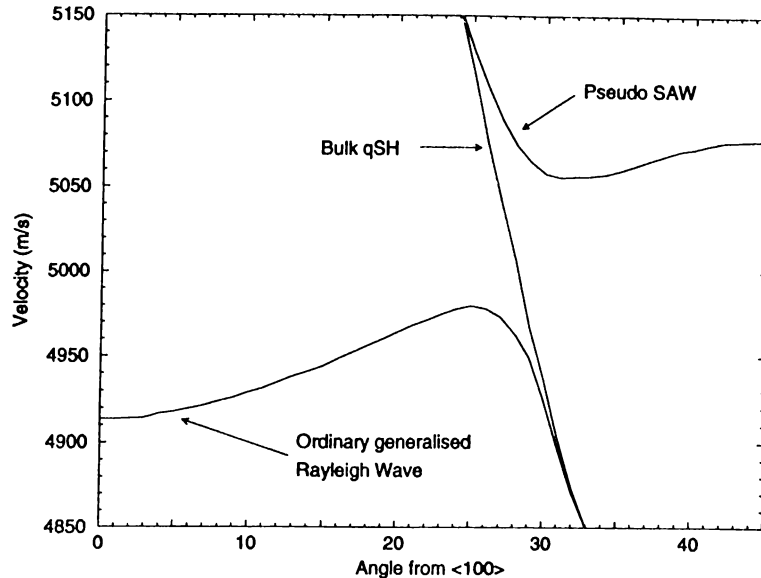
Figure 2.1: Calculated surface wave velocities on the [001] plane of silicon. Adopted from [21] .

length. This relation has a real root, the Rayleigh Root, which is approximately

$$\frac{V_{\mathrm{R}}}{V_s} \approx \frac{0.87 + 1.12\sigma}{1 + \sigma} \tag{2.2}$$

where σ is the Poisson ratio. When the medium is loaded with a liquid, power is coupled from the surface mode to the loading medium, causing a quasi-plane wave at an angle θ to the surface normal to propagate in the liquid. The propagation constant k of this wave satisfies the relation $k \sin \theta = \beta$, where β is the propagation constant of the Rayleigh wave. The surface wave will, hence, attenuate: its propagation constant is changed from β to $\beta - j\alpha$. This type of waves are known as leaky waves and α is the so-called leak rate. This leak mechanism forms the very essence of the $V(z)$ phenomena.

The Rayleigh velocity found in Eq. 2.2 is smaller than that of the slowest bulk mode in the material. This solution applies to isotropic materials. For anisotropic crystals, other wave modes exits together with the ordinary Rayleigh mode, for certain directions of the crystal structure. These modes are faster than the quasi-shear mode with highest velocity. As these waves attenuate due to coupling to bulk modes, they are called pseudo-surface modes [12]. For silicon, the ordinary Rayleigh mode velocity approaches to that of the bulk quasi-shear-horizontal (qSH) mode and then the pseudo-surface mode dominates, as illustrated in Fig. 2.1. A more detailed discussion on leaky waves is presented in App. A.

5

Determination of V_R from Acoustic Parameters

The reflection coefficient at the boundary of a liquid and an isotropic solid is given by [13]

$$R(k_x) = \frac{[(2k_x^2 - k_s^2)^2 - 4k_x^2\sqrt{(k_x^2 - k_l^2)(k_x^2 - k_s^2)}] - ik_s^4(\rho_w/\rho_s)\sqrt{(k_x^2 - k_l^2)/(k_w^2 - k_x^2)}}{[(2k_x^2 - k_s^2)^2 - 4k_x^2\sqrt{(k_x^2 - k_l^2)(k_x^2 - k_s^2)}] + ik_s^4(\rho_w/\rho_s)\sqrt{(k_x^2 - k_l^2)/(k_w^2 - k_x^2)}}$$

(2.3)

where k_x is the transverse wavenumber, ρ_s and ρ_w are the densities of the substrate and the coupling fluid, respectively. It has been shown [14] that, Eq. 2.3 has poles at $\pm k_p$ which are very close to $\pm k_R$, where k_R is the Rayleigh wavenumber and $k_p = \beta + j\alpha$. As the second term in the numerator has opposite sign with that in the denominator, $R(k_x)$ has zeros at $\pm k_0$, where k_0 is the complex conjugate of k_R. The variation of $R(k_x)$ for values of k_x close to k_R will be approximately

$$R(k_x) \approx \frac{k_x^2 - k_0^2}{k_x^2 - k_p^2}.$$

(2.4)

The reflection coefficient undergoes a phase shift of -2π as k_x increases past k_R. A good estimate for k_R is the value of k_x for which $\angle R(k_x) = -\pi$. For isotropic media, Eq. 2.3 can be used to determine the $-\pi$ phase crossing, by either directly evaluating the expression or using the Newton-Raphson algorithm to locate the zero of the denominator, the latter of which yields more accurate results. A typical example for the reflection coefficient is shown in Fig. 2.2. For anisotropic materials, the reflection coefficient has to be computed numerically to determine the leaky wave velocity [15].
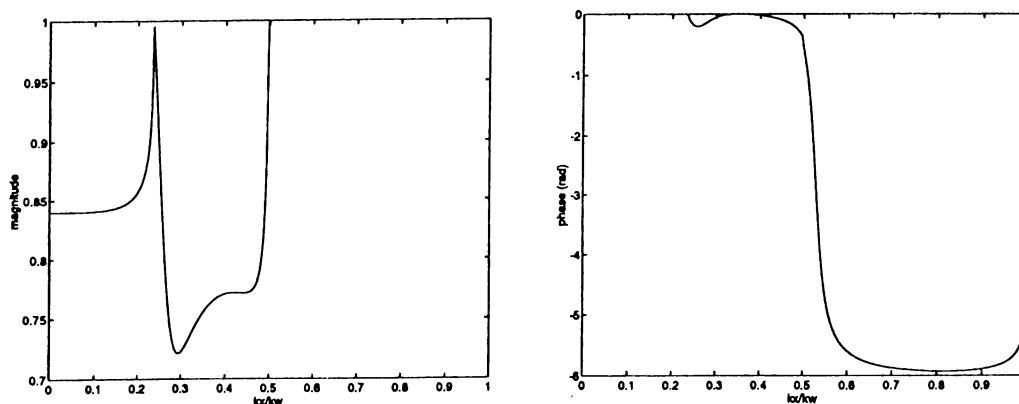
Figure 2.2: Reflection coefficient for an aluminium half space loaded with water.

2.2 Extraction of Leaky Wave Velocity

The conventional method of leaky wave velocity extraction from $V(z)$ data is based on the spectral analysis of the lens response. First, this method is described. Next, as an improvement in the extraction accuracy, a method using the $V(z)$ model developed for the V-groove lens is suggested.

2.2.1 V_R Extraction : Conventional Method

The conventional procedure [1] adapted for extracting SAW velocity from measured $V(z)$ data can be summarized as follows:

- Measure $V(z)$ for the object
- Obtain a $V_{ref}(z)$ using an object with no leaky wave generation at the V-groove excitation range.
- Find $V^2(z) - V_{ref}^2(z)$
- Filter out any unwanted interference frequencies
- Pad data with zeros
- Use a proper window function
- Apply FFT to find the period of oscillation
- Determine velocity from period

This method yields its best results if there is only one leaky wave mode. It is difficult to get accurate results particularly when there are two modes with close velocities. Unfortunately, many anisotropic materials support pseudo surface waves along particular directions [12] with a velocity very close to the SAW velocity. FFT algorithm gives biased results in such a case.

2.2.2 V_R Extraction : Model Based Method

The use of a model based algorithm introduces a considerable improvement in the SAW velocity extraction accuracy. This method involves the development of a model to reproduce the $V(z)$ and the extraction of material properties by fitting the model curve parameters.

A mathematical model regarding the response of the V-groove lens is developed for performance evaluation and leaky wave velocity extraction purposes.

7

The proposed model is based on geometric arguments and includes the effects of the acoustic parameters of the lens material, coupling fluid and the sample. Uniform insonifiction at the lens aperture is assumed and diffraction in the coupling fluid is ignored. In connection with the performance of the V-groove lens, the leaky wave excitation efficiency is demonstrated using the model. The derived $V(z)$ expressions are also employed in a model based algorithm as a refinement in the leaky wave velocity extraction accuracy.
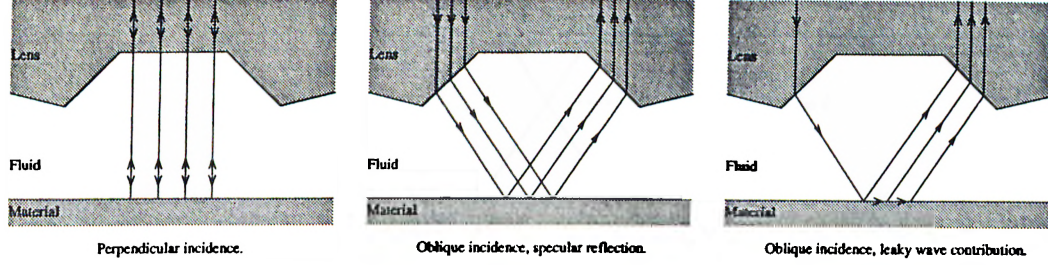
Figure 2.3: Reflection contributions to V(z).

The proposed V(z) model assumes that the output voltage is the absolute value of the sum of three complex terms (viz. Fig.2.3). The first term is due to the flat central portion of the V-groove lens. As this portion of the lens generates a beam that is perpendicularly incident on the material surface, its phase is assumed to be linearly dependent to the defocus distance. The second term arises from the specular reflection of the obliquely incident waves. The change in its phase depends on the inclination angle of the V-groove lens, as well as the defocus distance. The last term exists only if a leaky wave can be excited on the object surface. The phase of this term is assumed to depend on the critical angle of the object material. Since leaky waves decay exponentially, the amplitude of this term is exponentially dependent on the defocus distance.

The analysis for the development of the model is carried out for four distinct regions of defocus, whose boundaries are at $-\ell$, 0 and ℓ (Fig.2.4). Here, $\ell = \frac{f}{2\tan\theta_i}$, where θ_i is the incidence angle of the beam and f is the beamwidth measured along the horizontal axis. Region boundaries are basically determined by the presence or absence of each of the three components of the V(z). Essentially, the contribution of the central portion of the lens is always present, as long as the flat bottom of the groove is in perfect alignment with the material surface. The specular reflection and SAW contributions, on the other hand, are dependent on the amount of overlap of the sidebeams which are generated by the slanted edges of the groove.

The $z = 0$ reference for defocus is chosen as the location where the sidebeams perfectly overlap, or, in other words, the sample is at the focal plane

8
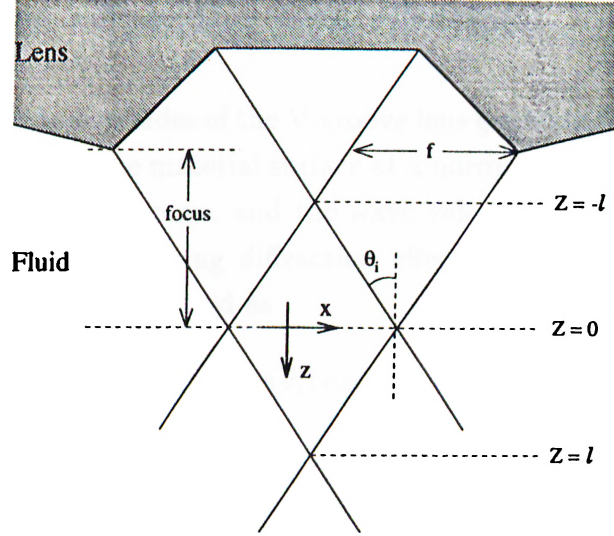
Figure 2.4: Geometric partitioning of the z-axis

of the lens (fig.2.4). The oblique specular contribution to $V(z)$ exist only for $-\ell < z < \ell$. As opposed to the case of specular reflection, SAW contribution is available for $z < -\ell$. Surely, the leaky wave contribution due to the sidebeams also ceases for $z > \ell$, for which the lens is completely out of focus. Throughout the derivations, the acoustic field is assumed to be uniform in the y direction. Phase terms due to propagation in z direction are introduced when the three contributions are combined. An $\exp(-j\omega t)$ time dependence is assumed.

Central Portion

The central portion of the V-groove lens generates a beam that is normally incident on the material surface. Ignoring diffraction, the incident field can be expressed as

$$p_{inc} = \exp[-\alpha_w z] \tag{2.5}$$

where α_w is the loss per unit length in the coupling fluid. Then, the reflected field is

$$p_{refl} = R(0)\exp[-\alpha_w z] \tag{2.6}$$

where $R(0)$ is the reflection coefficient at the material surface for normal incidence. Consequently [16],

$$V_1(z) = \int_{-\infty}^{\infty} p_{inc}(x)p_{refl}(x)dx \tag{2.7}$$

yielding

$$V_1(z) = V_1 \exp(-2\alpha_w z) \tag{2.8}$$

where V_1 is a constant determined by $R(0)$, the initial amplitude of the incident field, and the dimensions of the flat central portion.

9

Slanted Edges - Specular Contribution.

Each of the slanted planar sides of the V-groove lens generate a uniform acoustic field that is incident on the material surface at a normal angle of θ_i, determined by the inclination of the groove, and the wave velocities in the coupling fluid and the lens material. Ignoring diffraction effects, the incident field on the material surface can be expressed as

$$p_{inc}(x) = \begin{cases} \exp(-\alpha_w z/\cos\theta_i)\exp(jk_x x) & \text{for } -f < x < 0 \\ 0 & \text{elsewhere.} \end{cases} \tag{2.9}$$

Here f is the width of the beam measured along the x-axis, α_w is the loss per unit length in the coupling fluid, and k_x is the propagation constant along the x-axis. The reflected field is, then,

$$p_{refl}(x) = R(k_i)\exp(-\alpha_w z/\cos\theta_i)\exp(jk_x x) \tag{2.10}$$

where $R(k_i)$ is the specular (geometric) part of reflection coefficient for the particular incidence angle. The incident field from the edge through which the reflected field in Eqn. 2.10 reenters the lens is

$$p'_{inc}(x) = \begin{cases} \exp(-\alpha_w z/\cos\theta_i)\exp(-jk_x x) & \text{for } -f - 2z\tan\theta_i < x < -2z\tan\theta_i \\ 0 & \text{elsewhere} \end{cases} \tag{2.11}$$

Hence, the voltage at the transducer is

$$V(z) = \int_{-\infty}^{\infty} p_{refl}(x)p'_{inc}(x)dx = \int_{-\infty}^{\infty} R(k_i)p_{inc}(x)p'_{inc}(x)dx \tag{2.12}$$

Integral in eqn. 2.12 yields the following piecewise continuous expression for $V_2(z)$.

$$V_2(z) = \begin{cases} 0 & z < -\ell \\ V_2\exp(-2\alpha_w z/\cos\theta_i)(f + 2z\tan\theta_i) & -\ell < z < 0 \\ V_2\exp(-2\alpha_w z/\cos\theta_i)(f - 2z\tan\theta_i) & 0 < z < \ell \\ 0 & z > \ell \end{cases} \tag{2.13}$$

where V_2 is, again, a constant amplitude term determined by $R(k_i)$, the amplitude of the field at the back focal plane and the lens dimension.

Slanted Edges - Rayleigh Contribution.

As described above, the slanted planar edges of the V-groove lens generate a uniform acoustic field that is incident on the material surface at a normal angle of θ_i (fig.2.5). Again, ignoring diffraction effects, and choosing θ_i near
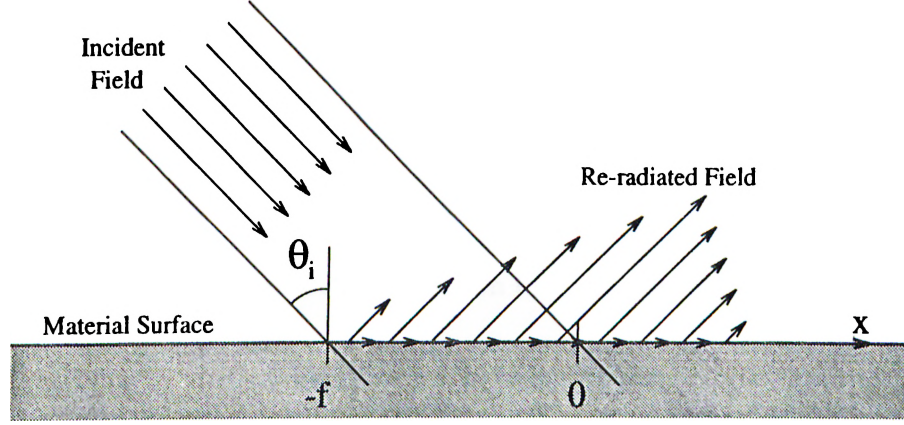
Figure 2.5: Leaky field pattern generated by the obliquely incident beam.

the Rayleigh critical angle θ_R, the incident field on the material surface can be expressed as

$$p_{inc}(x) = \begin{cases} \exp(jk_R x) & \text{for } -f < x < 0 \\ 0 & \text{elsewhere.} \end{cases} \qquad (2.14)$$

where k_R is the Rayleigh wavenumber. For a beam with an incidence angle near the Rayleigh critical angle, the re-radiated field is [13],

$$p_L(x) = -2\alpha_L \int_{-\infty}^{\infty} p_{inc}(x') \exp(jk_P |x - x'|) dx' \qquad (2.15)$$

where $k_P = k_R + j(\alpha_L + \alpha_D)$, and α_L and α_D are the leak and dissipation rates of the surface wave (see App. B for a derivation). Substituting $p_{inc}(x)$ into the above equation for $p_R(x)$ will yield the expressions for the leaky wave field (fig.2.5). For $x < -f$, there is no leaky wave propagation, hence lower limit of the integral is set to $-f$. Similarly, for $x > 0$, incident wave is zero. The integration, therefore, must be evaluated as

$$p_L(x) = -2\alpha_L \int_{-f}^{x''} \exp[jk_R x'] \exp[jk_P (x - x')] dx'. \qquad (2.16)$$

where

$$x'' = \begin{cases} x & \text{for } -f < x < 0 \\ 0 & \text{for } x > 0. \end{cases} \qquad (2.17)$$

11

Consequently, $p_L(x)$ can be found as

$$p_L(x) = \begin{cases} 0 & x < -f \\ -\frac{2\alpha_L}{\alpha_L + \alpha_D} \exp[jk_R x]\{1 - \exp[-(\alpha_L + \alpha_D)(f + x)]\} & -f < x < 0 \\ -\frac{2\alpha_L}{\alpha_L + \alpha_D} \exp[jk_R x] \exp[-(\alpha_L + \alpha_D)x]\{1 - exp[-(\alpha_L + \alpha_D)f]\} & x > 0 \end{cases}$$

$$(2.18)$$

$V(z)$ can now be formulated using geometric arguments proposed in the previous sections. The incident field on the material surface due to the edge through which the leaky field re-enters the lens is given by

$$p'_{inc}(x) = \begin{cases} \exp(-jk_x x) & \text{for } -f - 2z\tan\theta_i < x < -2z\tan\theta_i \\ 0 & \text{elsewhere} \end{cases}$$

$$(2.19)$$

The surface (Rayleigh) wave contribution to V(z), namely $V_3(z)$, is, then, given by

$$V_3(z) = \int_{-\infty}^{\infty} p_L(x)p'_{inc}(x)dx. \tag{2.20}$$

In order to be able to properly substitute the piecewise continuous expressions for $p_L(x)$ and $p'_{inc}(x)$, the above integral must be evaluated separately for each defocus region. For the sake of simplifying expressions, the attenuation in the coupling fluid is not included. For $z < -\ell$,

$$V_3'(z) = -\frac{2\alpha_L}{\alpha_L + \alpha_D}\{1 - \exp[-(\alpha_L + \alpha_D)f]\} \int_{-f-2z\tan\theta_i}^{-2z\tan\theta_i} \exp[-(\alpha_L + \alpha_D)x]dx$$

$$(2.21)$$

resulting in

$$V_3'(z) = -\frac{2\alpha_L}{(\alpha_L + \alpha_D)^2}\{1 - \exp[-(\alpha_L + \alpha_D)f]\}^2 \exp[-(\alpha_L + \alpha_D)(f + 2z\tan\theta_i)]$$

$$(2.22)$$

For $-\ell < z < 0$,

$$V_3'(z) = -\frac{2\alpha_L}{\alpha_L + \alpha_D}\left[\int_{-f-2z\tan\theta_i}^{0}\{1 - \exp[-(\alpha_L + \alpha_D)(f + x)]\}dx\right.$$

$$\left. + \{1 - \exp[-(\alpha_L + \alpha_D)f]\}\int_{0}^{-2z\tan\theta_i}\exp[-(\alpha_L + \alpha_D)x]dx\right]$$

$$(2.23)$$

which results in

$$V_3'(z) = -\frac{2\alpha_L}{(\alpha_L + \alpha_D)^2}[(f + 2z\tan\theta_i)(\alpha_L + \alpha_D)$$

$$+ \exp[-(\alpha_L + \alpha_D)f]\{1 - \exp[(\alpha_L + \alpha_D)(f + 2z\tan\theta_i)]\}$$

$$+ \{1 - \exp[-(\alpha_L + \alpha_D)f]\}\{1 - \exp[(\alpha_L + \alpha_D)]\}] \tag{2.24}$$

12

In the interval $0 < z < \ell$,

$$V_3'(z) = -\frac{2\alpha_L}{\alpha_L + \alpha_D} \int_{-f}^{-2z \tan \theta_i} \{1 - \exp[-(\alpha_L + \alpha_D)(f + x)]\} dx \qquad (2.25)$$

yielding

$$V_3'(z) = -\frac{2\alpha_L}{(\alpha_L + \alpha_D)^2}[(\alpha_L + \alpha_D)(f - 2z \tan \theta_i)$$

$$-\{1 - \exp[-(\alpha_L + \alpha_D)(f - 2z \tan \theta_i)]\}] \qquad (2.26)$$

Finally, for $z > \ell$, the lens is out of focus and hence,

$$V_3'(z) = 0. \qquad (2.27)$$

Including the attenuation in the coupling fluid, $V_3(z)$ is

$$V_3(z) = \exp\left(-\frac{2\alpha_w z}{\cos \theta_R}\right) V_3'(z) \qquad (2.28)$$

where $V_3'(z)$ is given by equations 2.22, 2.24, 2.26 and 2.27.

$V(z)$ model

Finally, the development of the $V(z)$ model for the V-groove lens requires to combine the three components constituting the overall lens response. The phase relations between the components are obtained from geometric arguments and the leaky wave velocity on the material surface.

$V_1(z)$ and $V_2(z)$, which are namely the geometric contributions to the lens response, combined will yield $V_{ref}(z)$, the model for the reference $V(z)$ output. As there is no leaky wave contribution in $V_{ref}(z)$, the reference output is based solely on the lens geometry. Therefore, fitting the model parameters to the actual reference curve is equivalent to tuning the model to the dimensions of the particular lens, which include the groove size and the inclination of the slanted edges.

While the phase gained by the beam due to the flat central portion of the groove is $k_w z$, where k_w is the wave number in the coupling fluid, the sidebeams encounter a phase change of $k_w z \cos \theta_i$ for a single trip from the lens aperture to the material surface. Taking into account the fact that the same distance is traveled once again after reflection from the material surface, the overall phase difference between $V_1(z)$ and $V_2(z)$ as a function of z turns out to be

$$4\pi z(1 - \cos \theta_i)\frac{1}{\lambda} \qquad (2.29)$$

13

where λ is the wavelength in the fluid, given by $\lambda = \frac{2\pi}{k_w}$. Consequently,

$$V_{ref}(z) = \left(V_1^2(z) + V_2^2(z) + 2V_1(z)V_2(z)\cos(4\pi z(1 - \cos\theta_i)\frac{1}{\lambda} + \psi_{12}) \right)^{1/2}$$

(2.30)

where ψ_{12} is constant phase term included to take care of the path length difference in the lens and the z-offset resulting from the choice of the origin for the z-axis, which is at the focal plane rather than the lens surface.

Once the expression concerning the lens geometry is derived, the effect of leaky waves can be introduced into the analysis. The phase gained by the leaky component is related to the Rayleigh critical angle of the particular material. Working with the square difference of $V(z)$ and $V_{ref}(z)$, rather than $V(z)$ itself, eliminates the cross terms containing $V_1(z)$ and $V_2(z)$, introducing a considerable simplification in the expressions. The resulting equation is

$$V^2(z) - V_{ref}^2(z) = V_3^2(z) \quad + \quad 2V_1(z)V_3(z)\cos(4\pi z(1 - \cos\theta_R)\frac{1}{\lambda} + \psi_3)$$

$$+ \quad 2V_2(z)V_3(z)\cos(4\pi z(\cos\theta_i - \cos\theta_R)\frac{1}{\lambda} + \psi_3 - \psi_{12})$$

(2.31)

where ψ_3 is the phase between $V(z)$ and $V_{ref}(z)$.

Leaky Wave Velocity Extraction : Model Based Method

To alleviate the problem caused by pseudo surface modes, an alternative procedure is proposed. A model based algorithm [17] is adopted, which suits better to the physical nature of the $V(z)$. The model curve is fitted to the actual $V(z)$ curve in the least mean square sense using Nelder-Mealde simplex search. As this particular search method is stable only in a close vicinity of the optimal solution, fairly good initial values for the model parameters are required. Therefore, the original $V(z)$ data is preprocessed to assure convergence. Furthermore, a rather simple model is selected to reduce computational complexity.

- Measure $V(z)$ for the object
- Obtain a $V_{ref}(z)$ as above
- Fit the model parameters to $V_{ref}(z)$ in the least mean square sense, using Nelder-Meade simplex search.

14

Reference Curve Parameters	
Parameter	Description
V_1	amplitude of $V_1(z)$
V_2	amplitude of $V_2(z)$
f	sidebeam width
θ_i	groove inclination angle
α_w	attenuation in the coupling fluid
ψ_{12}	phase between $V_1(z)$ and $V_2(z)$

$V^2(z) - V_{ref}^2(z)$ Parameters	
Parameter	Description
V_3	amplitude of $V_3(z)$
$\alpha_L + \alpha_D$	SAW leak rate
ψ_3	phase between $V_1(z)$ and $V_3(z)$
θ_R	Rayleigh critical angle

Table 2.1: Model parameters associated with the reference and square difference curves.

- Find $V^2(z) - V_{ref}^2(z)$
- Fit the model parameters using the same algorithm to the squared difference. Find the period of oscillation.
- Determine velocity from period

The extraction of leaky wave velocity involves a two step procedure. In the first step, the model parameters regarding the lens geometry are fitted to the reference response. There are six free model parameters for the geometric part: V_1 and V_2, the amplitudes of $V_1(z)$ and $V_2(z)$, respectively; f, width of the sidebeams; θ_i, the groove inclination angle; α_w, attenuation in the coupling fluid; and ψ_{12}, the phase between $V_1(z)$ and $V_2(z)$. The second step involves the optimization of the four parameters in the square difference expression. These are V_3, $\alpha_L + \alpha_D$, ψ_3 and θ_R. Nelder-Meade simplex search is used to fit the model curve to actual $V(z)$ and $V_{ref}(z)$ in the least mean square sense. Once θ_R is determined,

$$V_R = \frac{V_w}{\cos \theta_R} \tag{2.32}$$

relates the Rayleigh critical angle to the SAW velocity, where V_w is the acoustic wave velocity in the coupling fluid.

2.3 Design Considerations

Once the lens geometry is determined, the dimensions are to be optimized to meet design criteria on efficiency and bandwidth. The efficiency requirement on the design is dictated by the maximization of the leaky wave contribution to the $V(z)$ curve. This, in turn, leads to a high SNR, and, consequently, improves measurement accuracy. This maximization is desired to take place for those values of defocus for which $z < 0$, so that the major contribution to the output is from leaky waves, rather than the the geometric signal. For $z = -\ell$,

$$V_{\text{R}} \triangleq V_3'(z)|_{z=0} = -\frac{2\alpha_L}{(\alpha_L + \alpha_D)^2}\{1 - \exp[-(\alpha_L + \alpha_D)f]\}^2 \qquad (2.33)$$

due to eq. 2.22. Let V_I be the transducer output voltage when all of the field due to one of the slanted edges is reflected back to the lens and completely re-enters it through the opposite edge. Substituting $z = 0$ in eq. 2.13 and assuming the object is a perfect reflector, one finds $V_I = f$. Following the argument in [18], a good measure of efficiency is given by

$$\frac{V_{\text{R}}}{V_I} = -\frac{2\alpha_L}{f(\alpha_L + \alpha_D)^2}\{1 - \exp[-(\alpha_L + \alpha_D)f]\}^2 \qquad (2.34)$$

the maximum of which is attained for $f = 1.2564/(\alpha_L + \alpha_D)$. As an example, let $\alpha_D = 0$ and $\alpha_L = 2/\Delta_S$ where Δ_S is the Schoch displacement[14]. For this case we find

$$f/\Delta_S = 0.6282 \qquad \text{and} \qquad |V_{\text{R}}/V_I|_{max} = 0.8145.$$

For the optimum beamwidth, the loss of the lens is only 1.78 dB. This surprisingly low value of loss is due to the grooves resemblance to the wedge
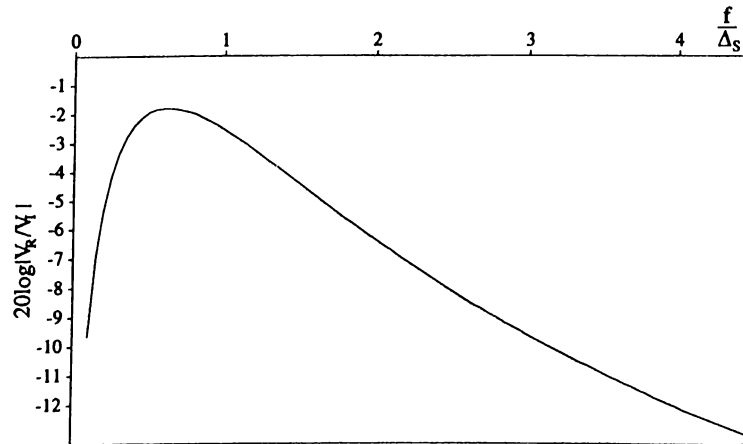

Figure 2.6: Normalized output voltage $(20 \log |V_{\text{R}}/V_I|)$ as a function of f/Δ_s.

16

transducer, whose inherent property is high coupling efficiency to leaky wave modes. Fig. 2.6 depicts $(20 \log |V_R/V_I|)$ as a function of f/Δ_s. The relatively flat peak indicates that the choice of the beamwidth is not extremely critical.
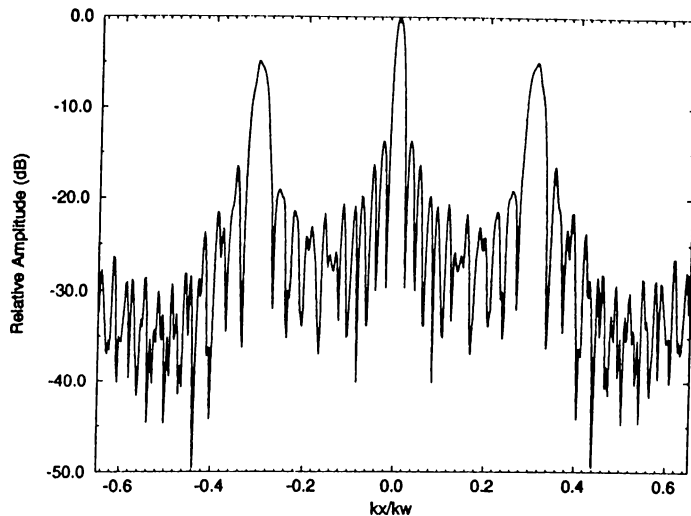

Figure 2.7: Angular spectrum of field at the aperture of an aluminium V-Groove lens with $l_1 = 1.5$mm., $l_2 = 3.2$mm. and $f = 23.8$ MHz.

One further concern regarding the aperture dimension is due to the angular beamwidth. The spectrum of the beam should be wide enough to be able to excite desired leaky modes in all directions for the particular crystal material. On the other hand, the beam should be confined to avoid coupling to unwanted wave modes. For silicon, the critical angle varies by 1 degrees for all directions. The angular spectrum of a rectangular aperture of width $2a$ is given by $F(\nu) = \text{sinc}(2a\nu) = \sin(2\pi a\nu)/2\pi a\nu$. The first zero of $F(\nu)$ is at $2\pi a\nu = \pi$ or $\nu = 1/2a$. To have a beam whose angular spectrum has a width of 2 degrees from zero to zero, one should chose $\lambda\nu = \sin(1°)$ or equivalently $2a \approx 60\lambda$. Figure 2.7 depicts the angular spectrum at the aperture of a lens designed for measurements on silicon. The two sidebeams have a -3 dB. width of 1.82 degrees.

The determination of the transducer-aperture spacing, d, is another critical issue in the design of a lens. There are three major sources of reflection for the case of the V-Groove Lens, as shown in figure 2.8. The first one is due to the flat central portion and is the strongest of all (which is numbered as "1" in the figure). Then pulses 2 and 3 are observed, which are reflections from the material surface from the perpendicular and obliquely incident beams, respectively. Their position in time with respect to the transmitted pulse varies with defocus and the interference of these generates the $V(z)$. Finally, a secondary echo from the aperture appears. The distance between the transducer

17
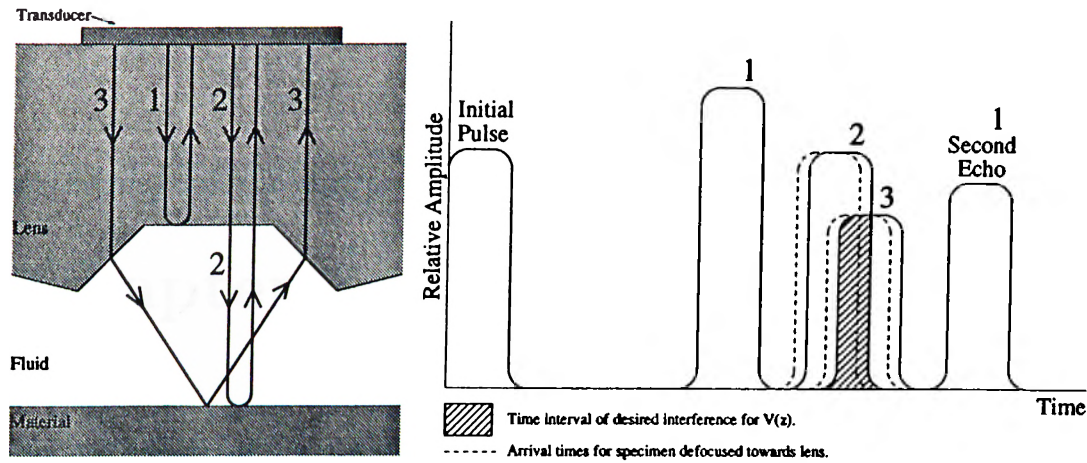
Figure 2.8: Reflections from various interfaces of the V-Groove lens (left) and associated time waveform (right). Graphics adopted from [1] .

and the aperture should be large enough so that the echoes from the material surface interfere with neither of these two pulses reflected from the lens-liquid boundary, for the whole working range of z.

A last point on the efficiency of the microscope system is the determination of the transducer size. The incident beam must be confined to the width of the aperture to cause minimum waste of power. For dimensions yielding a high Fresnel number, $N_F = a^2/\lambda d$, the diffraction pattern is very close to geometric shadow of the aperture. If $N_F < 0.5$, then the Fraunhofer approximation becomes applicable and the Fraunhofer diffraction pattern, which is indicated by the dashed line in fig. 2.9, can be used in computations regarding the transducer dimensions.

Aperture

Geometrical Shadow

- - - Width of Fraunhofer pattern in the far field
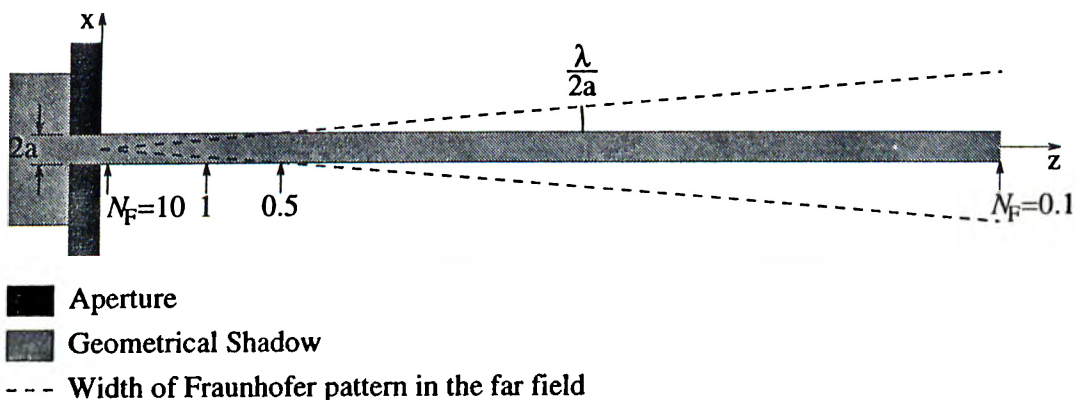
Figure 2.9: Fresnel diffraction from a slit of width $D = 2a$. N_F is the Fresnel number. Dashed line indicates the Fraunhofer diffraction pattern. Graphics adopted from [19] .

18

Chapter 3

SIMULATION

Simulating the performance of a lens involves propagation of acoustic waves between the transducer and the refracting element. The wavefront is then propagated through the refracting element using ray theory. The wave front is reflected from object surface upon propagation in liquid. This analysis is similar to the one developed for Lamb wave lens [6], except for the circular symmetry. While the circular symmetry of the Lamb lens allows the use of fast Hankel transform for propagation purposes, the propagation problem in V-groove lens requires the more costly two dimensional FFT.

The development of the simulation program starts with the determination of a region of interest, a rectangular area in the x-y plane outside of which the field is assumed to be zero. Next, the number of samples required in both horizontal directions are calculated. The x-component of wavevector k_x corresponding to the ith sample of the DFT coefficients is

$$k_x(i) = \frac{2\pi}{A} i \tag{3.1}$$

where A is the width of the region of interest, measured along the x-axis. To be able to include all propagating plane wave components of the field, i should run up to N_1 for which

$$k_x(N_1) = \frac{2\pi}{A} N_1 > k_w \tag{3.2}$$

is satisfied, where k_w is the wavenumber of the coupling fluid, which is greater than those of the lens and sample materials. Similarly, for the y-direction, the number of samples required is N_2, for which

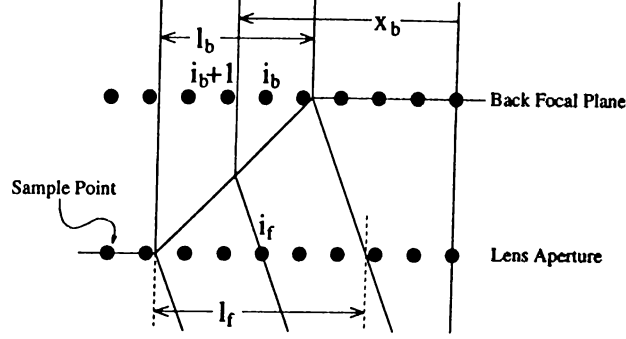$$\frac{2\pi}{B} N_2 > k_w \tag{3.3}$$

19

Figure 3.1: Determination of the effect of sidebeams to the field at the lens aperture.

holds, where B is the width of the region of interest along the y-axis.

The propagation of waves through a medium is achieved by multiplying each component of the 2-D DFT by proper phase and attenuation terms. If $U[i][j](z)$ denotes the DFT of the field at z, then

$$U[i][j](z_1) = U[i][j](z_0) \exp(-jk_z(i,j)z) \exp(-\alpha z k/k_z(i,j)) \qquad (3.4)$$

where

$$k_z(i,j) = \left(k^2 - k_x^2(i) - k_y^2(j) \right)^{1/2} \qquad (3.5)$$

provided $k_x^2(i) + k_y^2(j) > k^2$. Here k and α are the wavenumber and attenuation constant of the medium through which the wave is propagating, respectively. Plane wave components for which $k_z(i,j)$ is imaginary, $U[i][j](z_1) = 0$ as these correspond to evanescent modes. The wavefront at the lens aperture is determined using ray theory arguments. For the flat central portion of the lens, the field is simply multiplied with the transmission coefficient of the lens-liquid interface for perpendicular incidence, as this part does not introduce any refraction. For the slanted edges, first the sample points lying inside the area insonified by the sidebeams are determined. Next, for each point a ray is assumed to pass through. The value of each sample is set to the field value at the point from which this ray originates in the back focal plane. As it is likely that there is no sample point exactly at the location where the ray is passing, a weighted average of the nearest two samples is taken as the field value. Let x_b be the distance between the lens axis and the point in the back focal plane corresponding to the sample with index i_f in the aperture, as depicted in figure 3.2. The indices of the two samples in the back focal plane are, then, i_b and $i_b + 1$, where i_b is given by

$$i_b = \left\lfloor \frac{x_b}{\Delta x} \right\rfloor \qquad (3.6)$$

20

In the above expression, Δx is the sample spacing, i.e $\Delta x = A/N_1$. The field contribution of the sidebeam to the i_fth sample is then

$$u_3^+[i_f]_{sidebeam} = T(\phi)\left(\frac{l_b}{l_f}\right)^{1/2}\left[\left(\frac{x_b}{\Delta x} - i_b\right)u_2^+[i_b + 1] + \left(i_b + 1 + \frac{x_b}{\Delta x}\right)u_2^+[i_b]\right].$$

(3.7)

Here $T(\phi)$ is the transmission coefficient of the lens-liquid interface for an incidence angle ϕ, the inclination of the sidewalls. The square-rooted term is included for power conservation. Subscripts 2 and 3 indicate the wavefront at the back focal plane and the lens aperture, respectively.

Once $u_3^+[i][j]$s are determined, $V(z)$ can be computed using

$$V(z) = K \int_{-\infty}^{\infty}\int_{-\infty}^{\infty} U_3^+(k_x, k_y)U_3^-(-k_x, -k_y)dk_x dk_y$$

(3.8)

where K is an arbitrary scaling factor. In the simulation, first U_3^+ is to be computed. Then, this is to be propagated by a distance $d = f - z$ to find U_4^+, the angular spectrum of the field at the object surface. Here f is the focal length of the lens. Multiplying each component of U_4^+ with the proper reflection coefficient value, will yield U_4^-. This is, then, propagated back to the lens aperture, resulting in U_3^-. Replacing the integration with a summation, we have

$$
\begin{aligned}
V(z) &= \sum_{i=0}^{N-1}\sum_{j=0}^{N-1} U_3^+[i][j]U_3^-[-i][-j] \\
&= \sum_{i=0}^{N-1}\sum_{j=0}^{N-1} U_3^+[i][j]U_3^+[-i][-j]\exp(-2jk_z(i,j)d)\exp(-2\alpha dk/k_z(i,j))R[i][j]
\end{aligned}
$$

(3.9)

where $R[i][j] = R(k_x(i), k_y(j))$ is the reflection coefficient. The distance d in the phase and attenuation terms is multiplied with 2, as it is travelled twice.

Despite the lack of circular symmetry in the analysis of the V-groove lens, there are still some symmetry arguments which are useful in reducing the memory requirements of the simulation program and improving computation speed. The geometry is symmetric with respect to both the x and $y - axes$. This enables the reduction of array sizes by two for each dimension, hence the storage requirement for the field data decreases four times.

The symmetry in the field domain leads to similar arguments for the angular domain. Assuming that the symmetry axis for the filed data is chosen such
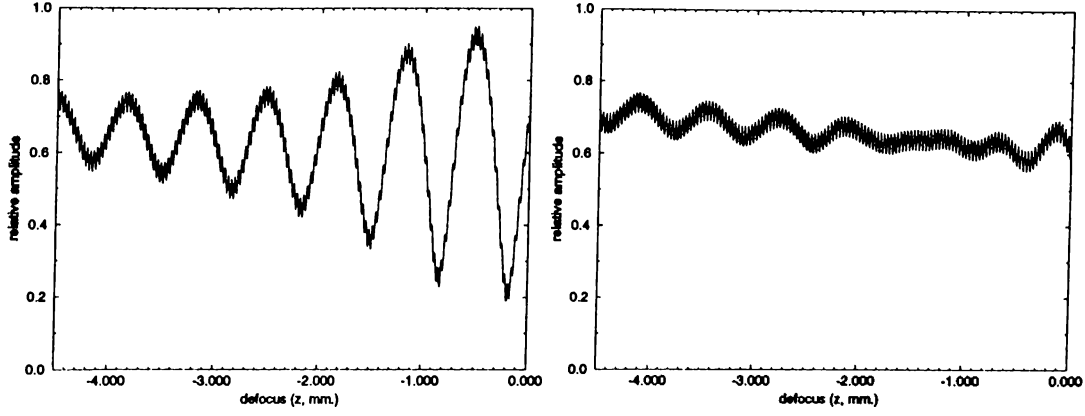
Figure 3.2: Sample outcome of the simulation program. The plot on the left is the $V(z)$ curve for the [001] plane of silicon, along 13° from [100]. The curve on the right depicts a reference curve, obtained using a steel halfspace.

that $u[-1-n] = u[n]$, then

$$
\begin{aligned}
U[-k] &= \sum_{n=<N>} u[n] \exp\left(-j\frac{2\pi}{N}(-k)n\right) \\
&= \sum_{n=<N>} u[-1-n] \exp\left(-j\frac{2\pi}{N}k(n+1)\right) \\
&= \underbrace{\sum_{n=<N>} u[n] \exp\left(-j\frac{2\pi}{N}kn\right)}_{U[k]} \exp\left(-j\frac{2\pi}{N}k\right)
\end{aligned}
\tag{3.10}
$$

so that

$$
U[-k] = U[N-k] = U[k]\exp\left(-j\frac{2\pi}{N}k\right). \tag{3.11}
$$

Equation 3.11 indicates that half of the field data is redundant. Coefficients $U[0]$ through $U\left[\frac{N}{2}-1\right]$ are sufficient to compute those ranging from $U\left[\frac{N}{2}+1\right]$ to $U[N]$. With the additional data point $U\left[\frac{N}{2}\right]$, all angular spectrum information can be held in an array of size $\frac{N}{2}+1$. For the two dimensional case, the array size is $\left(\frac{N_1}{2}+1\right) \times \left(\frac{N_2}{2}+1\right)$.

22

Chapter 4

EXPERIMENT

The performance of the V-groove lens was tested experimentally in our research laboratory. Fig. 4.1 depicts the set-up used throughout the experiments. The sample is placed in a water tank, which is placed over an X-Y tilt plane, for alignment purposes, and a rotation unit, to be used in direction sensitive measurements.

4.1 Measurement Electronics

The set-up used in experimentation performs the z-scan automatically under the control of an i8088 based personal computer via the parallel communication port and a IEEE 488 Bus Interface. The transmitted RF pulse is gated using a HP 8116 A, which is synchronized with the signal generator (HP 8656 B), making phased measurements possible. A second pulse generator is employed (HP 8112 A) to gate the echo signal. The time delay associated with this pulse is a function of defocus, as the time-of-flight of the RF pulse increases with z. An approximate formula for the time delay t_d is given by

$$t_d(z) = t_d(z_0) + 2 \left(\frac{1 + (\cos \theta_i)^{-1}}{2} \right) \left(\frac{z - z_0}{V_w} \right) \tag{4.1}$$

where $t_d(z_0)$ is the time delay set for z_0, the initial position of the lens and V_w is the wave velocity in the coupling liquid. The term $\left(1 + (\cos \theta_i)^{-1}\right)/2$ is included to set the delay to an average of the time delays required for the central beam and obliquely incident side beams, where θ_i is the incidence angle associated with them. The z-scan actuator is controlled by the computer with
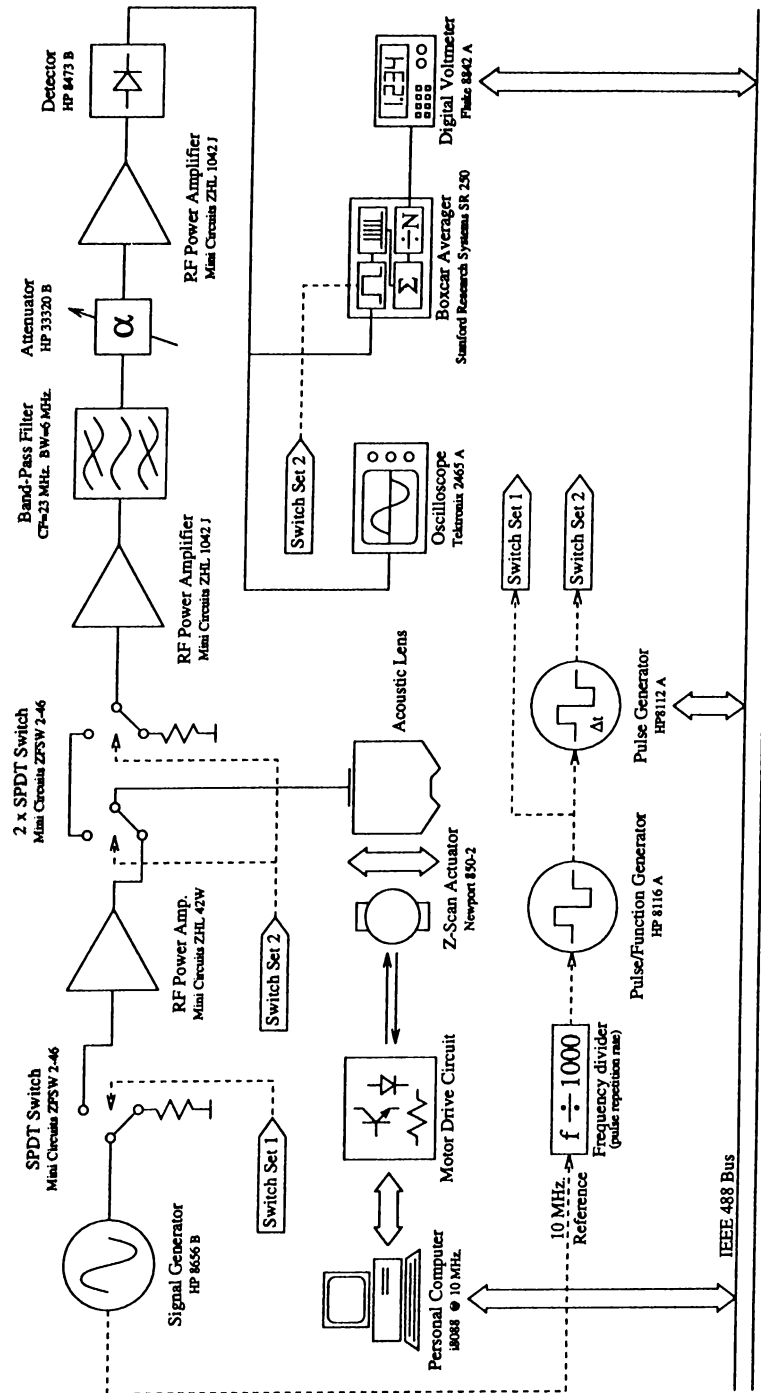
Figure 4.1: Experimental setup.

$0.2 \mu m.$ accuracy. As z is known to the computer, it is able to update the pulse delay using the approximate formula of eq.4.1.

Extreme care is taken in the RF electronics to maintain noise immunity. Low noise amplifiers are employed while necessary filtering blocks are inserted into the circuit. The RF leak signal due to the finite isolation of RF switches is minimized with the use of cascaded switches at the transmitter part.

4.2 The Lens

A V-groove lens is designed to measure surface acoustic wave velocity on silicon. Lens operates at 23.8 MHz. Lens dimensions are shown in fig 4.2. The silicon sample is a 525 microns thick silicon wafer. The Rayleigh wavelength
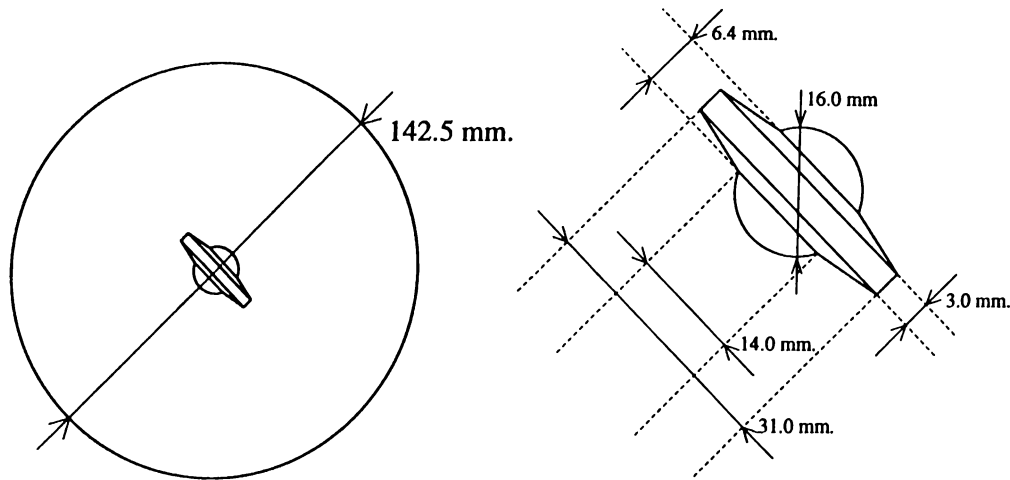
Figure 4.2: A to-scale drawing of the experimental lens (left) together with an enlarged view of the lens aperture showing its dimensions. The groove inclination is 22.9 deg. and aluminium block has a thickness of 49.0 mm.

is approximately 200 microns, and hence the wafer thickness is large enough for measurement purposes. Water temperature was stable within 0.5 degrees. The measured Rayleigh wave velocities are compensated against fluctuations in temperature. The alignment of the lens is achieved easily by maximizing the signal from the flat part of the lens, since the maximum signal is reached when the object surface is perfectly parallel to the flat part of V-groove. Experimental outcomes are presented in chapter 5.

A circular transducer with radius 5.0 mm is used to generate the acoustic beam. The lens-aperture spacing is 49.0 mm. The lens material is aluminium for which $V_l = 6420$ m/sec. The associated Fresnel number, $N_F = a^2/\lambda d$,

25

Transducer   Aperture
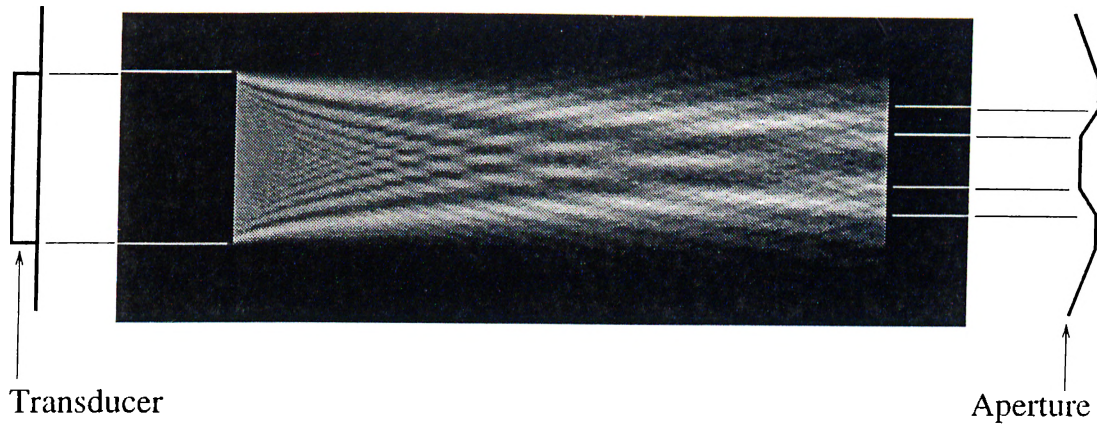
Figure 4.3: Intensity plot of acoustic field between transducer and aperture..
Transducer has width 10.0 mm and the travelled distance is 49.0 mm.

is then $N_{\mathrm{F}} = (10.0 \times 10^{-3}/2)^2/[(49.0 \times 10^{-3})(6420)/(23.8 \times 10^6)] = 1.89$. For
this value of N_{F}, the aperture is is essentially in the Fresnel region of the beam
generated by the transducer. Figure 4.3 indicates that the insonification at the
aperture is very close to the geometric shadow of the transducer, as expected.

Figure 4.4 shows the 2-dimensional angular spectrum at the aperture of
the lens used in the experiments. Three peeks are observed in the figure. The
central one corresponds to the perpendicularly incident beam while the other
two are due to the symmetrical side beams. The beamwidth of the later two
was found 1.82 degrees (fig.2.7).
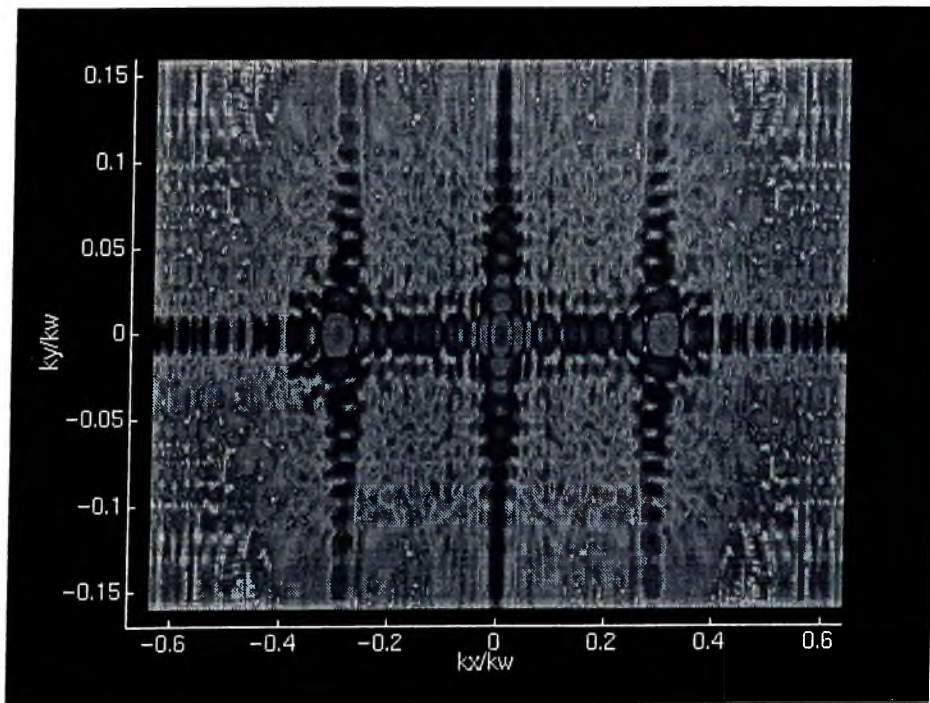
Figure 4.4: 2-dimensional angular spectrum at lens aperture in dB's.

26

Chapter 5

RESULTS

The performance of the V-groove lens has been evaluated by computer simulations and experimental studies. After a comment on the simulation program, we present a discussion on the leaky wave velocity measurement accuracy of the lens. Then, the efficiency of the lens is compared to other geometries. Finally, some experimental results are provided.

5.1   Simulations and Experiments

A simulation for the V-groove lens used in the experiments has been done. Fig. 5.1 depicts the simulation result together with the corresponding experi-

Figure 5.1: Calculated and measured $V(z)$ values for [001] cut Si.

mental $V(z)$ curve. The fit of the two curves is remarkable. The angle from [100] of the measurement direction is 13° for the [001] cut silicon sample. The

frequency of operation is 23.8 MHz. An aluminium lens is used in the experiments whose dimensions were provided in fig. 4.2.

5.2   Leaky Wave Velocity Extraction

The measurement accuracy of the V-groove lens has been tested by simulations. Leaky wave velocities have been extracted from $V(z)$ data for [001] surface of silicon along different directions using the F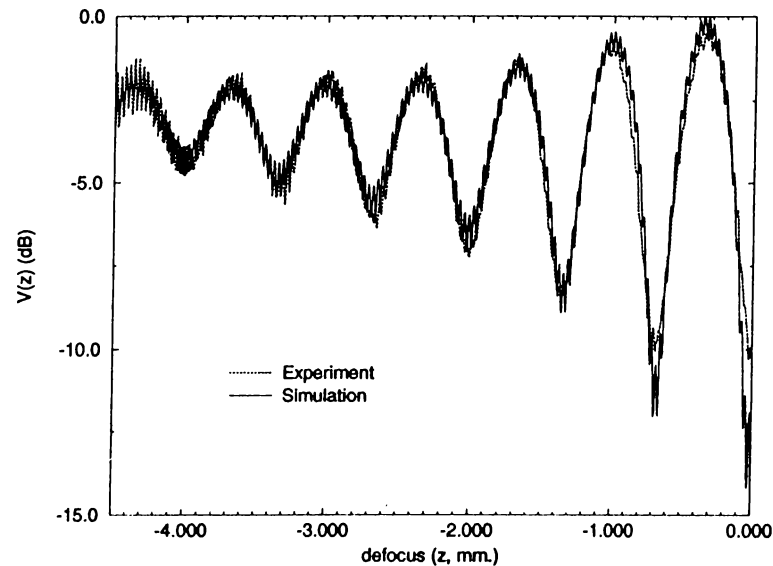FT method and the proposed model based algorithm. Results are given in fig. 5.2, together with calculated leaky wave velocities from elastic constants[20]. The extracted velocities using both
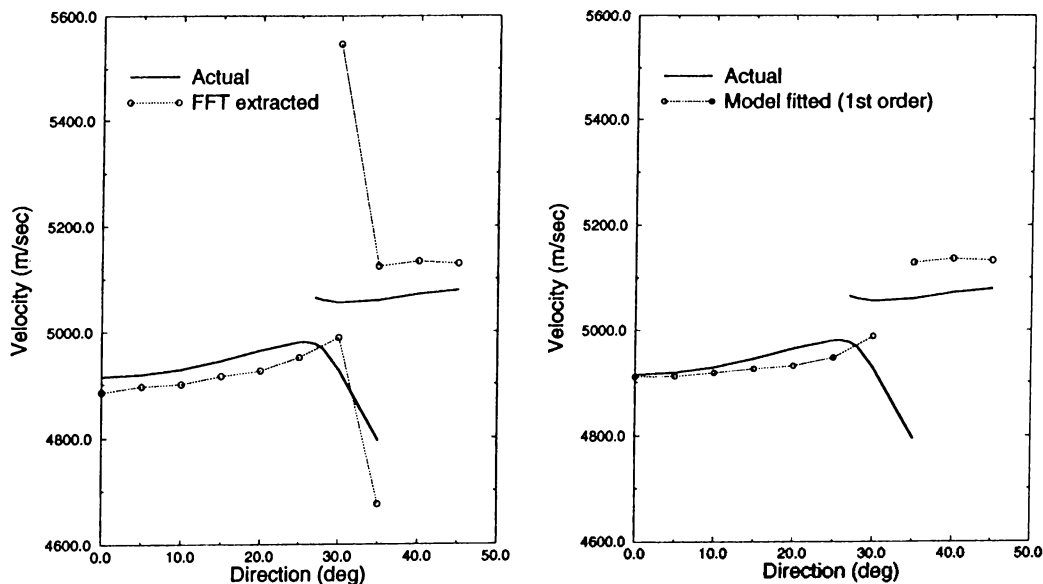
Figure 5.2: Calculated leaky wave velocities for the [001] surface of silicon together with measured values extracted using the FFT method (left) and the model based algorithm.

methods are within 1% of the values computed from elastic constants. The accuracy of the model based extraction is apparently better when there is no pseudo surface modes. Obviously, a single order method cannot match the inherent complexity of the data in the presence of pseudo surface modes.

To demonstrate accuracy of the proposed extraction method, example $V_{ref}(z)$ and $V^2(z) - V_{ref}^2(z)$ curves have been shown together with their respective fitted model curves (fig. 5.3). The sample is GaAs and the lens used has dimensions $l_2 = 65\mu m$, $l_1 = 33\mu m$. The frequency of operation is 400 MHz. Actual $V(z)$ and $V_{ref}(z)$ data are generated by the simulation program.

28

Figure 5.3: Example $V_{ref}(z)$ (left) and $V^2(z) - V_{ref}^2(z)$ (right) and their respective fitted model curves.

5.3 Performance of V-Groove Lens

To compare the performance of the V-groove lens to the LFB lens geometric and leaky wave parts of received signal is calculated for both geometry. Fig. 5.4 is plot of the results for the LFB lens, while fig. 5.5 shows the output of the V-Groove lens. Obviously, the geometric part is much greater for the latter. Leaky wave part is about 12 dB greater than LFB lens.
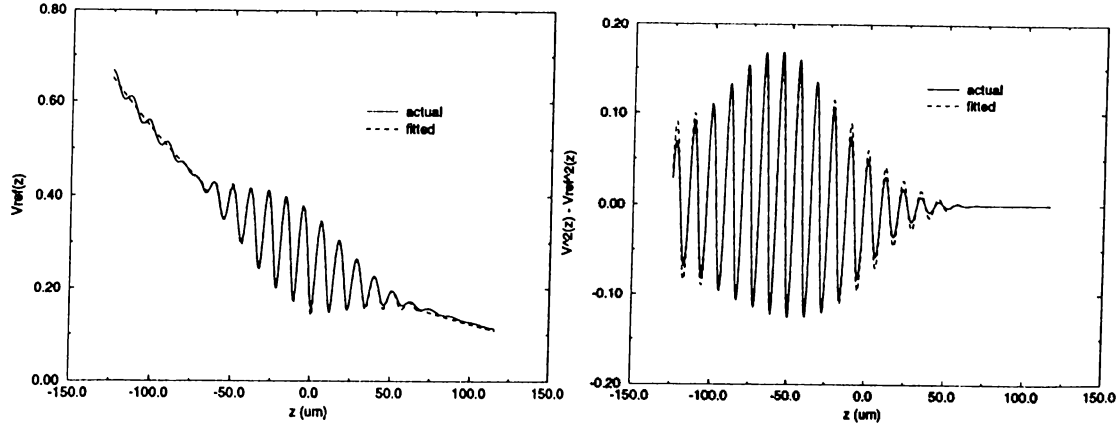
An immediate consequence of the efficiency of the V-groove lens is its accuracy of measurement, even for materials with high leaky wave velocities. A set of simulations with materials having a wide range of velocities has been done to demonstrate the absolute measurement accuracy. Table 5.1 shows the results for the LFB lens, while computations regarding the V-groove lens are tabulated in table 5.2. It is interesting to note that measured velocities for the V-groove lens are within 1% of their actual values, even for high velocity materials, while the accuracy of the LFB lens degrades as velocities increase.

Material	Actual	Uniform	Err.	Ideal	Err.	Pb Ref.	Err.
Aluminium	2858.6	2861.1	0.08%	2863.6	0.17%	2862.0	0.12%
Chromium	3656.7	3660.0	0.09%	3669.3	0.34%	3665.0	0.22%
Alumina	5679.0	5696.6	0.30%	5706.4	0.48%	5608.2	-1.25%
Si Carbide	6809.5	6850.1	0.60%	6884.8	1.11%	6672.4	-2.01%

Table 5.1: Absolute errors using LFB lens for different materials under different assumptions. Actual velocities (first column) are compared with $V(z)$ extracted velocities under uniform field (second column), real field with ideal reference reflector (fourth column), real field with Pb as reference reflector (sixth column) assumptions.

Material	Actual	Uniform	Err.	Ideal	Err.	Pb Ref.	Err.
Aluminium	2858.6	2854.3	-0.15%	2848.8	-0.34%	2846.3	-0.43%
Chromium	3656.7	3654.0	-0.07%	3650.3	-0.18%	3642.9	-0.38%
Alumina	5679.0	5665.6	-0.24%	5636.3	-0.75%	5659.3	-0.35%
Si Carbide	6809.5	6810.5	0.01%	6792.3	-0.25%	6741.7	-0.98%

Table 5.2: Absolute errors using V-groove lens for different materials under different assumptions. Actual velocities (first column) are compared with $V(z)$ extracted velocities under uniform field (second column), real field with ideal reference reflector (fourth column), real field with Pb as reference reflector (sixth column) assumptions.

Figure 5.4: Calculated geometrical and leaky wave parts of $V(z)$ for LFB lenses designed for copper and alumina objects (f=500 MHz). For the first lens $r = 70$ μm, and For the second $r = 120$ μm.
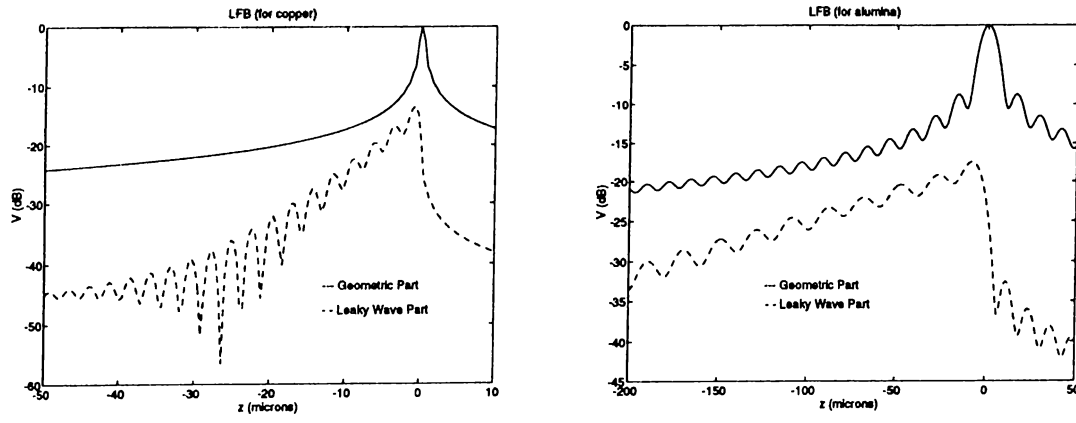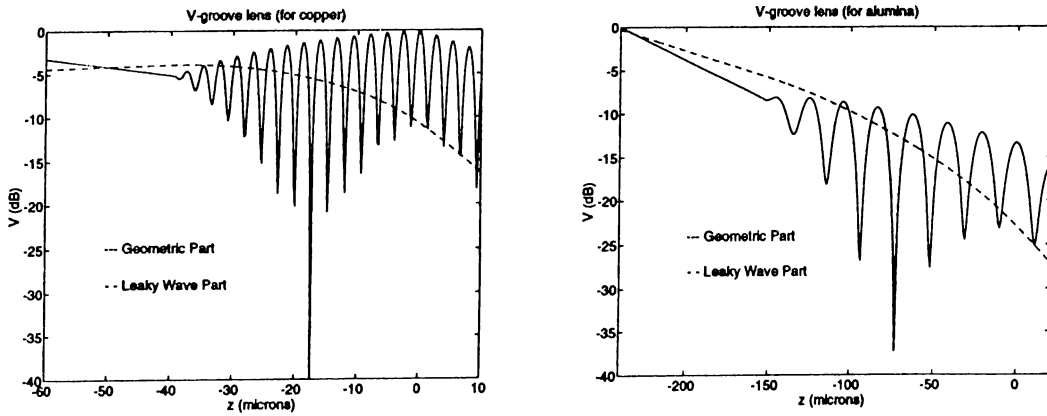

Figure 5.5: Calculated geometrical and leaky wave parts of $V(z)$ for V-groove lenses designed for copper and alumina objects (f=500 MHz). For the first lens $l_1 = 25$ μm, $l_2 = 70$ μm. For the second lens $l_1 = 40$ μm, $l_2 = 120$ μm. Diffraction effects are neglected

30

Actual V_R (m/s)	Groove Mismatch	Extracted V_R (m/s)	Error (%)
4474.0	-0.6 °	4487.3	0.2973
4474.0	-0.4 °	4484.6	0.2369
4474.0	-0.2 °	4483.5	0.2123
4474.0	0.0 °	4477.2	0.0715
4474.0	+0.2 °	4473.9	-0.0022
4474.0	+0.4 °	4466.7	-0.1632
4474.0	+0.6 °	4458.4	-0.3487

Table 5.3: Simulation results for a V-groove lens with $l_1 = 33\mu m$, $l_2 = 65\mu m$. The simulations are done for the (011) surface of silicon as the reflector and the operation frequency was $400MHz$.

The measurement accuracy of the V-groove lens is dependent on the match between the median direction of the refracted beam and the critical angle of the material. Nevertheless, this dependence does not introduce a significant degradation in the accuracy of the extracted velocity. As long as the critical angle of the material is within the interval of angular spectrum to which the refracted beam is confined, the error is less than $\pm 1\%$. Table 5.3 shows the performance of the V-groove lens for various mismatch values.

5.4 Experimental Results

A set of experiments on [011] cut silicon has been performed to measure the leaky wave velocity for directions in 1° steps. Steel is used as the material for reference curve measurements. A sample $V(z)$ curve is presented in fig. 5.6.
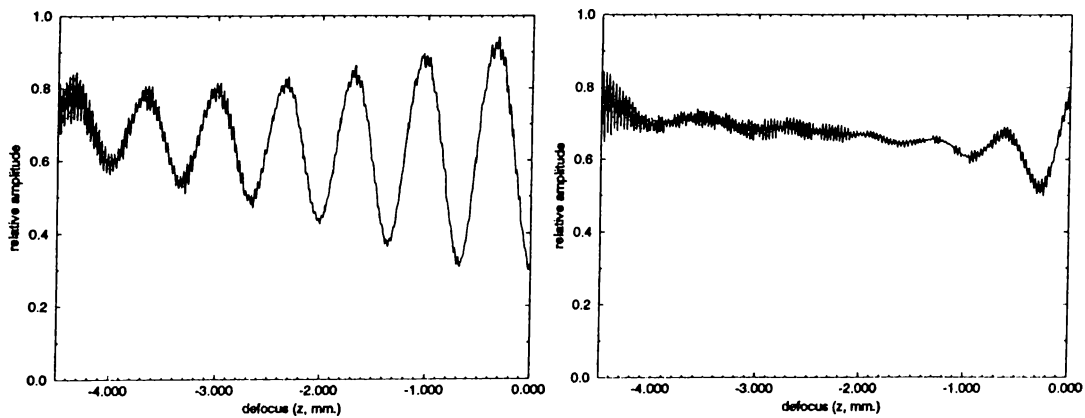

Figure 5.6: Experimental $V(z)$ curve obtained from the [001] plane of silicon, at 13° from [100] (left), and a reference curve measured using a steel substrate.

The resulting velocity measurements are depicted in fig. 5.7 together with theoretical figures obtained directly from elastic parameters and simulation results.

The experimental results match the theoretical values with absolute error less than 0.5%, except for the transition region around 25° from [100]. The temperature variations during the measurements are recorded and the experimental velocities are computed in accordance with these values. The theoretical values are determined from the $-\pi$ phase crossing of the reflection coefficient and the FFT method was used in the extraction of leaky wave velocities from the $V(z)$ curves generated by the simulation program.
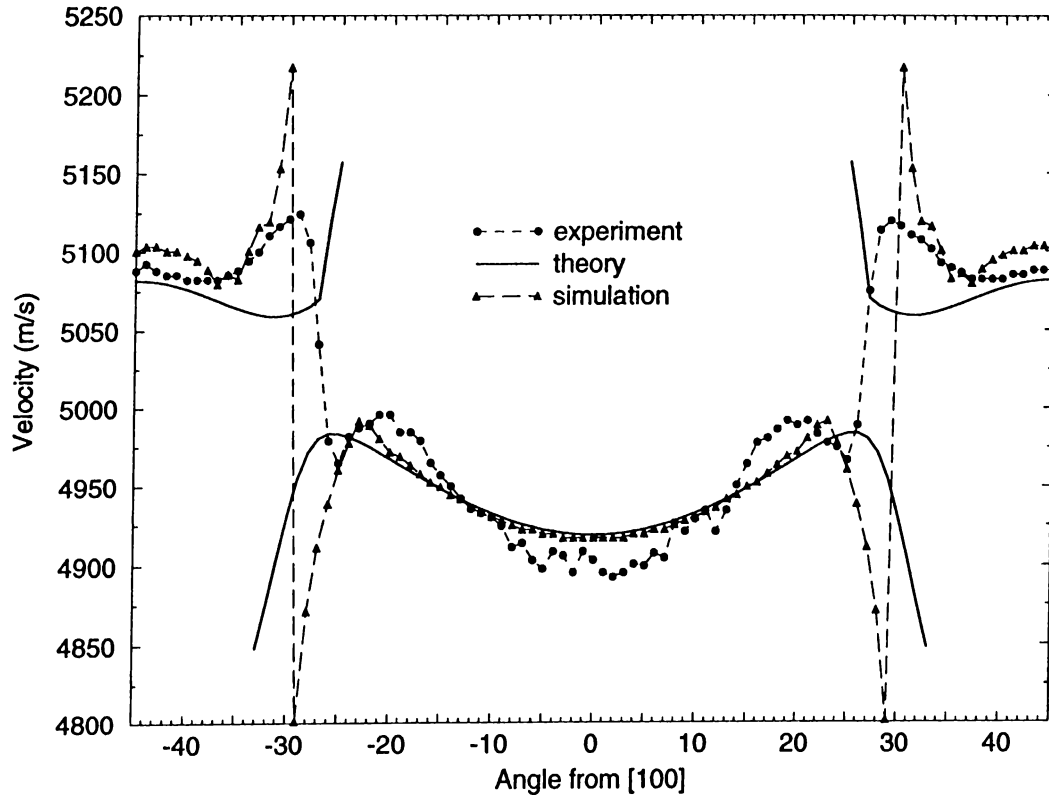
Figure 5.7: Experimental results together with theoretically computed leaky wave velocities for [011] cut silicon. The sample was $525\mu m$. thick and the operation frequency was 23.8 MHz.

Tabulated elastic constants for silicon are used in the computation of wave velocities. This is one of the major reasons for the mismatch between the theoretical values and experimental results. The elastic constants of the sample may not match the tabulated figures.

The accuracy of the wave velocity in the coupling fluid used in the computations is another critical issue, affecting the reliability of the measurement. One way to compute V_w, the wave velocity in water, is to use the temperature of water[1]. Another method is to make use of the finite leak of the switches. The interference between the leak RF and the return echo causes wiggles to appear on the $V(z)$ curve, as seen in Fig. 5.6 The period of this high frequency

32

signal is given by $V_w/2f$ $(m.)$, from which V_w can be determined using spectral analysis. Here f is the frequency of operation. This method has been employed to determine the water velocity for each measured $V(z)$ data of the experiment. The relevant region of the spectrum is plotted in Fig. 5.8. The amount of leak for angles ranging from -30 degrees to 30 degrees is insufficient for a reliable measurement. Nevertheless. for those angles for which the peak is apparent (the dark area around 0.31). V_w can be predicted satisfactorily. The accuracy of this method has been tested by simulations and it turns out to be very good if the amount of leak is reasonable.
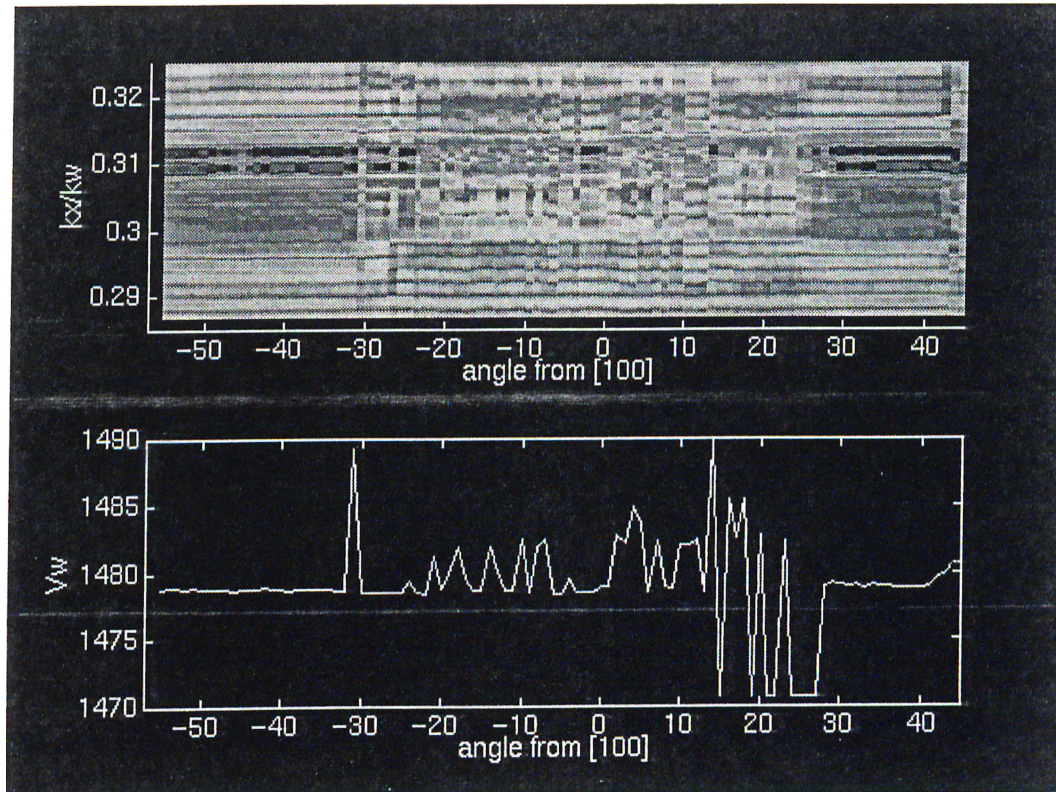

Figure 5.8: Spectral plot of $V(z) - V_{ref}(z)$ covering the region of interference caused by leaky switches (above) and resulting V_w measurement (below).

Chapter 6

CONCLUSION

The proposed V-groove lens is proved to be a power tool in the characterization of anisotropic materials. It has direction sensitivity comparable to the LFB lens, while its leaky wave excitation efficiency is as good as that of the Lamb wave lens. The former makes the geometry suitable for the determination of direction dependent acoustic parameters and the later implies accurate measurements. The V-groove lens maintains a large signal level and modulation index over a wide range of defocus values. This ability is desirable particularly for materials with high leaky wave velocities. As the number of oscillations in the $V(z)$ curve is limited for these materials, the measurement accuracies of conventional lens geometries are low. The V-groove lens, as opposed to these, has an absolute measurement accuracy of 1% for materials with a wide range of leaky wave velocities.

The conventional method for leaky wave extraction is based on the spectral analysis of the sampled $V(z)$ curve using DFT. This particular method leads to erroneous results in the presence of multiple leaky wave modes. As a remedy, a model based approach was proposed. This method, makes use of physical arguments regarding the operation of the lens to work out the $V(z)$ curve. The model based curve is then fitted to the actual one by optimizing the parameters describing the lens output. Considerable improvement in accuracy was observed with the use of the model based method for the case of isotropic solids. Unfortunately, measurements for materials with multiple leaky wave modes is still problematic. The model needs a refinement to incorporate the effects of pseudo surface modes.

The dimensions of a V-groove lens need to be optimized to yield best performance in terms of accuracy and efficiency. This has to be done taking into consideration the acoustic parameters of the specimen. Once the lens is tuned for a particular material, it cannot be employed in measurements on any other material whose critical angle for leaky modes does not match the incidence angle of the beam generated by the lens. A lens designed for silicon cut along its [001] plane will not work even for the [011] surface of the same material. However, a slight mismatch between the median direction of incident beam and the critical angle does not cause a significant degradation in the performance. The error is less than 0.5% as long as the spectrum of the beam covers the critical angle.

The developed simulation program was extensively used to test the performance of the V-groove lens. Using plane wave decomposition for propagation purposes and employing ray theory arguments for the refracting elements, the program was able to produce quite accurate results. Features like leaky wave extraction accuracy, angular spectrum of lens output an the insonification pattern of the acoustic transducer were evaluated using the program.

Experimentation on V-groove lens indicates that the expectancies on accuracy and efficiency are valid. A lens fabricated using equipment with very limited precision yields results that meet the theoretically expected resolution and matches simulations very nicely, as well. This result is due to the inherent suitability of the geometry to its objective, well established analysis methods and a delicate electronics supporting the measurement system. Together with these, the careful evaluation of design parameters resulted in a prototype that produced quite striking results.

This exhaustive study on the V-groove lens showed that the proposed geometry meets all predicted specifications on its performance. This new powerful lens is a challenging tool in the qualitative evaluation of materials with crystallographic anisotropies and it is hoped that it will be merited in accordance, in the literature.

Appendix A

LEAKY WAVES

This appendix provides the reader with information regarding Rayleigh waves, which are surface wave modes that exist at the boundary of a solid halfspace and leaky waves, that are the modified form of surface waves when the solid is loaded with a semi-infinite liquid (adopted from [11]).

A.1 Rayleigh Waves

Consider a solid, semi-infinite in the $-y$ direction, for which the particle displacement is assumed to be in y and z directions (Fig. A.1). As the motion
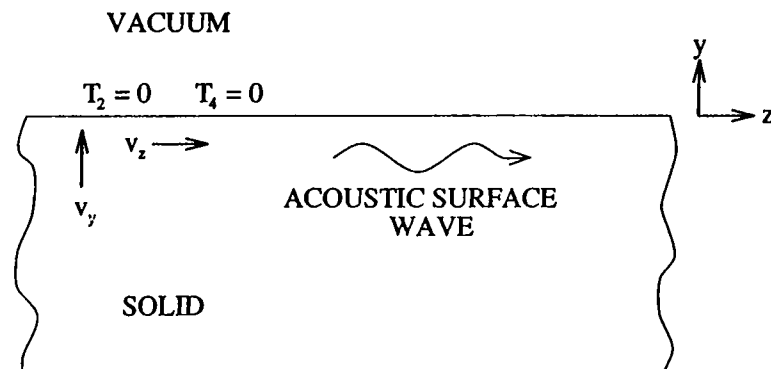

Figure A.1: Configuration for acoustic surface wave analysis.

is independent of the coordinate x, the vector potential is given by $\Psi = a_x \psi$. Potentials ϕ and ψ are associated with the longitudinal and shear components

of motion, respectively. The following equations can be written:

$$u_z = \frac{\partial \phi}{\partial z} - \frac{\partial \psi}{\partial y} \tag{A.1}$$

$$u_y = \frac{\partial \phi}{\partial y} + \frac{\partial \psi}{\partial z} \tag{A.2}$$

$$T_1 = \lambda \left(\frac{\partial^2 \phi}{\partial y^2} + \frac{\partial^2 \phi}{\partial z^2} \right) \tag{A.3}$$

$$T_2 = \lambda \left(\frac{\partial^2 \phi}{\partial y^2} + \frac{\partial^2 \phi}{\partial z^2} \right) + 2\mu \left(\frac{\partial^2 \phi}{\partial y^2} + \frac{\partial^2 \psi}{\partial y \partial z} \right) \tag{A.4}$$

$$T_3 = \lambda \left(\frac{\partial^2 \phi}{\partial y^2} + \frac{\partial^2 \phi}{\partial z^2} \right) + 2\mu \left(\frac{\partial^2 \phi}{\partial z^2} - \frac{\partial^2 \psi}{\partial y \partial z} \right) \tag{A.5}$$

$$T_4 = \mu \left(2\frac{\partial^2 \phi}{\partial y \partial z} + \frac{\partial^2 \psi}{\partial z^2} - \frac{\partial^2 \psi}{\partial y^2} \right) \tag{A.6}$$

Wave equations for potentials are give by

$$\frac{\partial^2 \phi}{\partial z^2} + \frac{\partial^2 \phi}{\partial y^2} + k_l^2 \phi = 0 \tag{A.7}$$

and

$$\frac{\partial^2 \Psi}{\partial z^2} + \frac{\partial^2 \Psi}{\partial y^2} + k_s^2 \Psi = 0 \tag{A.8}$$

where k_l and k_s are wave numbers. Shear and longitudinal components are expected to have the same phase variation in the z direction. Hence,

$$\phi = F(y)e^{j(\omega t - \beta z)} \tag{A.9}$$

$$\psi = G(y)e^{j(\omega t - \beta z)} \tag{A.10}$$

Substituting these into their respective wave equations yield

$$\frac{d^2 F}{dy^2} = (\beta^2 - k_l^2)F(y) \tag{A.11}$$

$$\frac{d^2 G}{dy^2} = (\beta^2 - k_s^2)G(y) \tag{A.12}$$

We are looking for solutions that fall off exponentially in the $-y$ direction as these waves have finite energy stored per unit length. We choose $F(y)$ and $G(y)$ to vary as $\exp(\gamma_l y)$ and $\exp(\gamma_s y)$, respectively. It follows that $\gamma_l^2 = \beta^2 - k_l^2$ and $\gamma_s^2 = \beta^2 - k_s^2$. Therefore,

$$\phi = Ae^{j\beta z}e^{\gamma_l y} \tag{A.13}$$

$$\psi = Be^{j\beta z}e^{\gamma_s y} \tag{A.14}$$

As the solid is in vacuum, the normal component of stress at the surface must be zero. Substituting the expressions onf ϕ and ψ into the stress equations and

settin $T_2 = 0$ and $T_4 = 0$ yields

$$B = -\frac{2j\beta\gamma_l A}{\beta^2 + \gamma_s^2}$$

(A.15)

and

$$A = \frac{2j\beta\gamma_s B}{\beta^2 + \gamma_s^2}$$

(A.16)

The last two equations, when combined, result in a form of Rayleigh wave dispersion relation, namely

$$4\beta^2\gamma_l\gamma_s - (\beta^2 + \gamma_s^2)^2 = 0$$

(A.17)

This equation has a real root, the *Rayleigh root*, which is approximately

$$\frac{k_s}{\beta} = \frac{V_R}{V_s} \approx \frac{0.87 + 1.12\sigma}{1 + \sigma}$$

(A.18)

where $V_R = \omega/\beta$, V_s is the shear wave velocity and σ is the Poisson ratio.

A.2 Leaky Waves

Now consider the case when the semi-infinite medium is loaded with a liquid. Here, it is assumed that a wave can propagate in the liquid with a phase velocity lower than that of the surface wave. If a surface wave is excited on the surface of the solid, than it is expected that this excites a quasi-plane in the liquid at an angle θ to the normal. For this wave $k \sin \theta = \beta$, where k is the propagation constant in the liquid (Fig. A.2). Under these conditions, the surface wave continuously radiates power into the loading medium. Hence, the propagation constant is changed from β to $\beta - j\alpha$, where α is the leak rate.
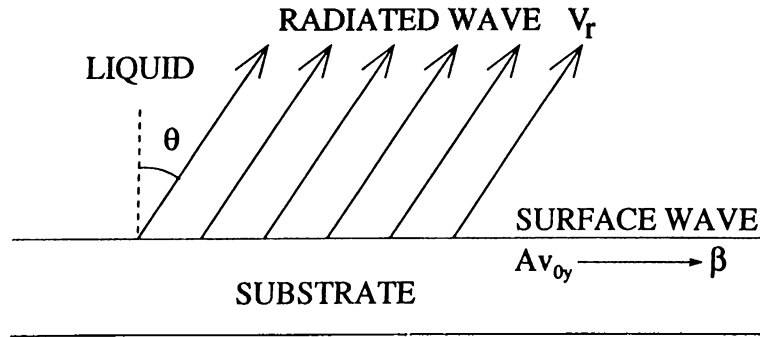

Figure A.2: Leaky surface wave radiating into a liquid.

The boundary conditions at the surface of the solid are perturbed due to the presence of the loading medium, so that the normal component of stress is

38

no longer zero. Assuming the width of the acoustic beam is w and the field is uniform in the x direction, we have

$$\frac{dA}{dz} + j\beta A = \frac{w}{4} v_{0y}^* \hat{T}_2 \qquad (A.19)$$

due to perturbation theory. Here, T_2 is the component of stress normal to the substrate and v_{0y} is the velocity normalized to unity power at $y = 0$ of the unperturbed Rayleigh wave. The particle velocity in the y direction $\hat{v}_y$, associated with the Rayleigh wave, is defines as

$$\hat{v}_y = A v_{0y} \qquad (A.20)$$

In this solution, while the boundary conditions on $\hat{v}_y$ are used, Eq. A.19 is employed to account for the change in the boundary condition for T_2. Assuming that the radiated wave has particle velocity $\hat{v}$ in a direction θ to the surface normal, we have

$$\hat{v}\cos\theta = A v_{0y} \qquad (A.21)$$

The stress in a liquid is invariant with angle. Thus

$$\hat{T}_2 = -Z_L \hat{v} = \frac{-Z_L A v_{0y}}{\cos\theta} \qquad (A.22)$$

It follows from Eqs. A.19-A.22 that

$$\frac{dA}{dz} + j\beta A = -\alpha A \qquad (A.23)$$

where

$$\alpha = \frac{w v_{0y} v_{0y}^* Z_L}{4\cos\theta} \qquad (A.24)$$

The solution of Eq. A.23 is

$$A(z) = A_0 e^{-(j\beta+\alpha)z} \qquad (A.25)$$

where A_0 is the amplitude of the wave at $z = 0$. The value of v_{0y} can be found from the Rayleigh wave solution given in Sec. A.1. This is the postulated leaky wave.

Appendix B

COMPUTATION OF THE RE-RADIATED FIELD

The reflection coefficient $R(k_x)$ at a solid-liquid interface can be factorized, so that

$$R(k_x) = R_0(k_x)R_R(k_x) \approx R_0(k_x)\frac{k_x^2 - k_0^2}{k_x^2 - k_p^2} = R_0(k_x)\left(1 + \frac{k_p^2 - k_0^2}{k_x^2 - k_p^2}\right) \qquad (B.1)$$

where $R_R(k_x)$ describes the behavior of $R(k_x)$ around the Rayleigh pole. Here, k_p is the location of the Rayleigh pole in the complex k_x plane. The fraction $(k_p^2 - k_0^2)/(k_x^2 - k_p^2)$ in Eq. B.1 contributes significantly only when $|k_x|$ is close to $|k_p|$. As $|R(k_x)| = 1$ for $k_x \geq k_s > \mathrm{Re}\, k_p$, we may write

$$R(k_x) \approx R_0(k_x) + \frac{k_p^2 - k_0^2}{k_x^2 - k_p^2}. \qquad (B.2)$$

Here, the second term on the right describes the Rayleigh pole singularity. If $P_{inc}(k_x)$ is the Fourier transform of $p_{inc}(x)$, the incident field, then the reflected field can be found by taking the inverse Fourier transform of the product of $P_{inc}(k_x)$ and $R(k_x)$. If the reflected field is separated into geometric and Rayleigh wave parts, i.e

$$p_{ref}(x) = p_G(x) + p_R(x) \qquad (B.3)$$

which can be computed using the separation of $R(k_x)$. The geometric part is

$$p_G(x) = \frac{1}{2\pi}\int_{-\infty}^{\infty} R_0(k_x)P_{inc}(k_x)\exp(jk_x x)dk_x \qquad (B.4)$$

and the Rayleigh component is

$$p_R(x) = \frac{1}{2\pi}\int_{-\infty}^{\infty} \frac{k_p^2 - k_0^2}{k_x^2 - k_p^2}P_{inc}(k_x)\exp(jk_x x)dk_x. \qquad (B.5)$$

The $p_{inc}(k_x)$ term in the integrand can be written in term of the spatial field by a further integration. The Rayleigh component is, then

$$p_R(x) = \frac{1}{2\pi} \int_{-\infty}^{\infty} p_{inc}(x') \left\{ \int_{-\infty}^{\infty} \frac{k_p^2 - k_0^2}{k_x^2 - k_p^2} \exp\left[jk_x(x - x')\right] dk_x \right\} dx'. \qquad (B.6)$$

When the effect of the fluid can be regarded as a light perturbation on the propagation of Rayleigh waves on the surface of the solid, so that $\alpha_R \ll k_R$, then

$$\frac{j(k_p^2 - k_0^2)}{2k_p} \approx -2\alpha_R. \qquad (B.7)$$

The re-radiated field is then

$$p_R(x) = -2\alpha_R \int_{-\infty}^{\infty} p_{inc}(x') \exp\left[jk_x|x - x'|)\right] dx'. \qquad (B.8)$$

Here α_R is the leak rate of the surface wave and k_R is the propagation constant of the unperturbed Rayleigh wave. This analysis is adopted from [1].

REFERENCES

[1] A. Briggs. *Acoustic Microscopy.* Oxford University Press, Oxford, 1992.

[2] R.A. Lemons and C.F. Quate "A scanning acoustic microscope," in *Proc. IEEE 1973 Ultrasonics Symposium,* pp. 18–20, 1973.

[3] C.F. Quate, A. Atalar, and H.K.Wickramasinghe "Acoustic microscopy with mechanical scanning — a review," *Proc. of the IEEE,* vol. 67, pp. 1092–1114, 1979.

[4] A. Atalar, C.F. Quate, and H.K. Wickramasinghe "Phase imaging with the acoustic microscope," *Appl. Phys. Lett.,* vol. 31, pp. 791–793, 1977.

[5] J. Kushibiki, A. Ohkubo, and N. Chubachi "Anisotropy detection in sapphire by acoustic microscope using line-focus beam," *Elect. Lett.,* vol. 17, pp. 534–536, 1981.

[6] A. Atalar and H. Köymen "A high efficiency lamb wave lens for subsurface imaging," in *Proc. of IEEE 1989 Ultrasonics Symposium,* pp. 813–816, 1989.

[7] A. Bozkurt, G. Yaralıoğlu, A. Atalar, and H. Koymen "A new directional acoustic lens: V-groove lens," in *IEEE Ultrasonic Proceedings,* 1993.

[8] R.D. Weglein "A model for predicting acoustic material signatures," *Appl. Phys. Lett.,* vol. 34, pp. 179–181, 1979.

[9] W. Parmon and H.L. Bertoni "Ray interpretation of the material signature in the acoustic microscope," *Elect. Lett.,* 1979.

[10] A. Atalar "A physical model for the acoustic signatures," *J. Appl. Phys.,* vol. 50, pp. 8237–8239, 1979.

[11] G.S. Kino. *Acoustic Waves: Devices, Imaging and Analog Signal Processing.* Prentice-Hall, Englewood Cliffs, 1987.

[12] T.C. Lim and G.W. Farnell "Character of pseudo surface waves on anisotropic crystals," *J. Acoust. Soc. Am.*, vol. 45, pp. 845–851, 1969.

[13] H.L. Bertoni "Ray-optical evaluation of v(z) in the reflection acoustic microscope," *IEEE Trans. Son. Ultrason.*, vol. 31, pp. 105–116, 1984.

[14] H.L. Bertoni and T. Tamir "Unified theory of rayleigh angle phenomena for acoustic beams at liquid—solid interfaces," *Appl. Phys.*, vol. 2, pp. 157–172, 1973.

[15] O. Arıkan, E. Teletar, and A. Atalar "Reflection coeficient null of acoustic waves at a liquid-anisotropic-solid interface," *J. Acoust. Soc. Am.*, vol. 85, pp. 1–10, 1989.

[16] A. Atalar "A backscattering formula for acoustic transducers," *J. Appl. Phys.*, vol. 51, pp. 3093–3098, 1980.

[17] S.L. Marple Jr. *Digital Spectral Analysis with Applications.* Prentice-Hall, Englewood Cliffs, 1987.

[18] A. Atalar and H. Köymen "Use of a conical axicon as a surface acoustic wave focusing device," *IEEE Trans. Ultrason. Ferroelect. and Freq. Control*, vol. 34, pp. 53–63, 1987.

[19] B.E.A. Saleh and M.C. Teich. *Fundamentals of Photonics.* Wiley, New York, 1991.

[20] B.A. Auld. *Acoustic Fields and Waves in Solids*, volume 1. Wiley, New York, 1973.

[21] Zenon Sklar. *Quantitative Acoustic Microscopy of Coated Materials.* PhD thesis, Wolfson College, University of Oxford, Trinity term 1993.